PHOTONIC-CRYSTAL OPTICS

Felix Bloch (1905–1983) developed a theory that describes electron waves in the periodic structure of solids.

Eli Yablonovitch (born 1946) coinvented the concept of the photonic bandgap; he made the first photonic bandgap crystal.

Sajeev John (born 1957) invoked the notion of photon localization and was a coinventor of the photonic bandgap idea.

243

The propagation of light in homogeneous media and its reflection and refraction at the boundaries between different media are a principal concern of optics, as described in the earlier chapters of this book. Photonic devices often comprise multiple layers of different materials arranged, for example, to suppress or enhance reflectance or to alter the spectral or the polarization characteristics of light. Multilayered and stratified media are also found in natural physical and biological systems and are responsible for the distinct colors of some insects and butterfly wings. Multilayered media can also be periodic, i.e., comprise identical dielectric structures replicated in a one-, two-, or three-dimensional periodic arrangement, as illustrated in Fig. 7.0-1. One-dimensional periodic structures include stacks of identical parallel planar multi-layer segments. These are often used as gratings that reflect optical waves incident at certain angles, or as filters that selectively reflect waves of certain frequencies. Two-dimensional periodic structures include sets of parallel rods as well as sets of parallel cylindrical holes, such as those used to modify the characteristics of optical fibers known as holey fibers (see Chapter 9). Three-dimensional periodic structures comprise arrays of cubes, spheres, or holes of various shapes, organized in lattice structures much like those found in natural crystals.
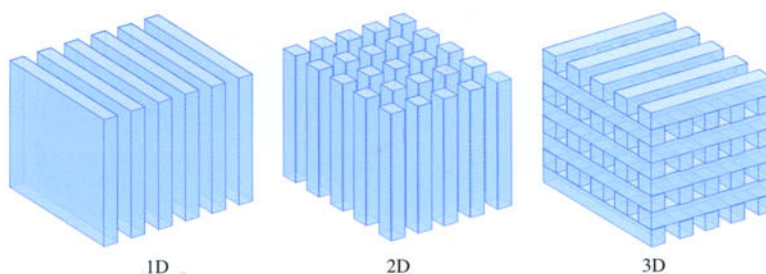

Figure 7.0-1 Periodic photonic structures in one-dimensional (1D), two-dimensional (2D), and three-dimensional (3D) configurations.

Optical waves, which are inherently periodic, interact with periodic media in a unique way, particularly when the scale of the periodicity is of the same order as that of the wavelength. For example, spectral bands emerge in which light waves cannot propagate through the medium without severe attenuation. Waves with frequencies lying within these forbidden bands, called **photonic bandgaps**, behave in a manner akin to total internal reflection, but applicable for all directions. The dissolution of the transmitted wave is a result of destructive interference among the waves scattered by elements of the periodic structure in the forward direction. Remarkably, this effect extends over finite spectral bands, rather than for just single frequencies.

This phenomenon is analogous to the electronic properties of crystalline solids such as semiconductors. The periodic wave associated with an electron travels in a periodic crystal lattice, and energy bandgaps are commonly found. Because of this analogy, the photonic periodic structures have come to be called **photonic crystals**. Photonic crystals have found many applications, including use as special filters, waveguides, and resonators, and many more applications are in the offing.

An electromagnetic-optics analysis is usually required to describe the optical properties of inhomogeneous media such as multilayered and periodic media. For inhomogeneous dielectric media, as we know from Sec. 5.2B, the permittivity $\epsilon(\mathbf{r})$ is spatially varying and the wave equation takes the general forms of (5.2-16) and (5.2-17). For a harmonic wave of angular frequency ω, this leads to generalized Helmholtz equations

244

for the electric and the magnetic fields expressed as

$$\eta(\mathbf{r}) \, \nabla \times (\nabla \times \mathbf{E}) = \frac{\omega^2}{c_o^2} \mathbf{E}, \tag{7.0-1}$$

$$\nabla \times [\eta(\mathbf{r}) \, \nabla \times \mathbf{H}] = \frac{\omega^2}{c_o^2} \mathbf{H}, \tag{7.0-2}$$

**Generalized
Helmholtz Equations**

where $\eta(\mathbf{r}) = \epsilon_o/\epsilon(\mathbf{r})$ is the electric impermeability (see Sec. 6.3A). One of these equations may be solved for either the electric or the magnetic field, and the other field may be directly determined by use of Maxwell's equations. Note that (7.0-1) and (7.0-2) are cast in the form of an eigenvalue problem: a differential operator applied on the field function equals a constant multiplied by the field function. The eigenvalues are ω^2/c_o^2 and the eigenfunctions provide the spatial distributions of the modes of the propagating field (see Appendix C). For reasons to be explained in Secs. 7.2C and 7.3, we work with the magnetic-field equation (7.0-2) instead of the electric-field equation (7.0-1).

For multilayered media, $\epsilon(\mathbf{r})$ is piecewise constant, i.e., it is uniform within any given layer but changes from one layer to another. Wave propagation can then be studied by using the known properties of optical waves in homogeneous media, together with the appropriate boundary conditions that dictate the laws of reflection and transmission.

Periodic dielectric media are characterized by periodic values of $\epsilon(\mathbf{r})$ and $\eta(\mathbf{r})$. This periodicity imposes certain conditions on the optical wave. For example, the propagation constant deviates from simply proportionality to the angular frequency ω, as is the case for a homogeneous medium. While the modes of propagation in a homogeneous medium are plane waves of the form $\exp(-j\mathbf{k} \cdot \mathbf{r})$, the modes of the periodic medium, known as **Bloch modes**, are traveling waves modulated by standing waves.

This Chapter

Previous chapters have focused on the optics of thin optical components that are well separated, such as thin lenses, planar gratings, and image-bearing films across which the light travels. This chapter addresses the optics of *bulk* media comprising multiple dielectric layers and periodic 1D, 2D, and 3D photonic structures. Section 7.1, in which 1D layered media are considered, serves as a prelude to periodic media and photonic crystals. A matrix approach offers a systematic treatment of the multiple reflections that occur at the multiple boundaries of the medium. Section 7.2 introduces photonic crystals in their simplest form — 1D periodic structures. Matrix methods are adopted to determine the dispersion relation and the band structure. An alternative approach, based on a Fourier-series representation of the periodic functions associated with the medium and the wave, is also presented. These results are generalized in Sec. 7.3 to two- and three-dimensional photonic crystals.

Throughout this chapter, the various media are assumed to be isotropic, and therefore described by a scalar permittivity ϵ, although reflection and refraction at boundaries have inherent polarization-sensitive characteristics.

Photonic Crystals in Other Chapters

By virtue of their omnidirectional reflection property, photonic crystals can be used as "perfect" dielectric mirrors. A slab of homogeneous medium embedded in a photonic crystal may be used to guide light by multiple reflections from the boundaries.

Applications to optical waveguides are described in Sec. 8.4. Similarly, light may be guided through an optical fiber with a homogeneous core embedded in a cladding of the same material, but with cylindrical holes parallel to the fiber axis. Such "holey" fibers, described in Sec. 9.4, have a number of salutary features not present in ordinary optical fibers. A cavity burrowed in a photonic crystal may function as an optical resonator since it has perfectly reflecting walls at frequencies within the photonic bandgap. Photonic-crystal microresonators will be described briefly in Secs. 10.4D and 17.4C.

7.1   OPTICS OF DIELECTRIC LAYERED MEDIA

A. Matrix Theory of Multilayer Optics

A plane wave normally incident on a layered medium undergoes reflections and transmissions at the layer boundaries, which in turn undergo their own reflections and transmissions in an unending process, as illustrated in Fig. 7.1-1(a). The complex amplitudes of the transmitted and reflected waves may be determined by use of the Fresnel equations at each boundary (see Sec. 6.2); the overall transmittance and reflectance of the medium can, in principle, be calculated by superposition of these individual waves. This technique was used in Sec. 2.5B to determine the transmittance of the Fabry–Perot interferometer.
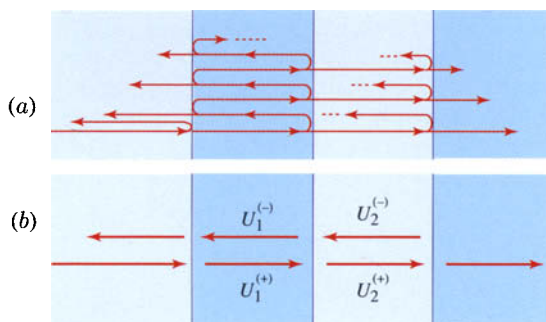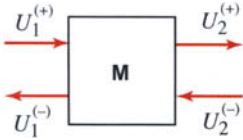

(a)

(b)

Figure 7.1-1 (a) Reflections of a single wave from the boundaries of a multilayered medium. (b) In each layer, the forward waves are lumped into a forward collected wave $U^{(+)}$, and the backward waves are lumped into a backward collected wave $U^{(-)}$.

In layer 1: $U_1^{(-)}$, $U_1^{(+)}$. In layer 2: $U_2^{(-)}$, $U_2^{(+)}$.

When the number of layers is large, tracking the infinite number of "micro" reflections and transmissions can be tedious. An alternative "macro" approach is based on the recognition that within each layer there are two types of waves: forward waves traveling to the right, and backward waves traveling to the left. The sums of these waves add up to a single forward collected wave $U^{(+)}$ and a single backward collected wave $U^{(-)}$ at any point, as illustrated in Fig. 7.1-1(b). Determining the wave propagation in a layered medium is then equivalent to determining the amplitudes of this pair of waves everywhere. The complex amplitudes of the four waves on the two sides of a boundary may be related by imposing the appropriate boundary conditions, or by simply using the Fresnel equations of reflection and transmission.

Wave-Transfer Matrix

Tracking the complex amplitudes of the forward and backward waves through the boundaries of a multilayered medium is facilitated by use of matrix methods. Consider two arbitrary planes within a given optical system, denoted plane 1 and plane 2. The amplitudes of the forward and backward collected waves at plane 1, $U_1^{(+)}$ and $U_1^{(-)}$,

respectively, are represented by a column matrix of dimension 2, and similarly for plane 2. These two column matrices are related by the matrix equation

$$\begin{bmatrix} U_2^{(+)} \\ U_2^{(-)} \end{bmatrix} = \begin{bmatrix} A & B \\ C & D \end{bmatrix} \begin{bmatrix} U_1^{(+)} \\ U_1^{(-)} \end{bmatrix}. \qquad (7.1\text{-}1)$$

The matrix **M**, whose elements are A, B, C, and D, is called the **wave-transfer matrix** (or **transmission matrix**). It depends on the optical properties of the layered medium between the two planes.

A multilayered medium is conveniently divided into a concatenation of basic elements described by known wave-transfer matrices, say $\mathbf{M}_1$, $\mathbf{M}_2$,..., $\mathbf{M}_N$. The amplitudes of the forward and backward collected waves at the two ends of the overall medium are then related by a single matrix that is the matrix product,
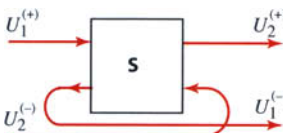

$$\mathbf{M} = \mathbf{M}_N \dots \mathbf{M}_2 \mathbf{M}_1, \qquad (7.1\text{-}2)$$

where the elements $1, 2, \dots, N$ are numbered from left to right as shown in the figure. The wave-transfer matrix cascade formula provided in (7.1-2) is identical to the ray-transfer matrix cascade formula given in (1.4-10), and it proves equally useful:

Scattering Matrix

An alternative to the wave-transfer matrix that relates the four complex amplitudes $U_{1,2}^{(\pm)}$ at the two edges of a layered medium is the scattering matrix, or **S** matrix. It is often used to describe transmission lines, microwave circuits, and scattering systems. In this case, the outgoing waves are expressed in terms of the incoming waves,
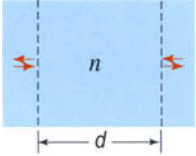

$$\begin{bmatrix} U_2^{(+)} \\ U_1^{(-)} \end{bmatrix} = \begin{bmatrix} t_{12} & r_{21} \\ r_{12} & t_{21} \end{bmatrix} \begin{bmatrix} U_1^{(+)} \\ U_2^{(-)} \end{bmatrix}, \qquad (7.1\text{-}3)$$

where the elements of the **S** matrix are denoted t_{12}, r_{21}, r_{12}, and t_{21}. Unlike the wave-transfer matrix, these elements have direct physical significance. The quantities t_{12} and r_{12} are the forward amplitude transmittance and reflectance (i.e., the transmittance and reflectance of a wave incident from the left), respectively, while t_{21} and r_{21} are the amplitude transmittance and reflectance in the backward direction (i.e., a wave coming from the right), respectively. The subscript 12, for example, signifies that the light is incident from medium 1 into medium 2. This can be easily verified by noting that if there is no backward wave at plane 2, so that $U_2^{(-)} = 0$, we obtain $U_2^{(+)} = t_{12}U_1^{(+)}$ and $U_1^{(-)} = r_{12}U_1^{(+)}$. Similarly, if there is no forward wave at plane 1, so that $U_1^{(+)} = 0$, we obtain $U_2^{(+)} = r_{21}U_2^{(-)}$ and $U_1^{(-)} = t_{21}U_2^{(-)}$.

A distinct advantage of the **S**-matrix formalism is that its elements are directly related to the physical parameters of the system. On the other hand, a disadvantage is that the **S** matrix of a cascade of elements is not the product of the **S** matrices of the constituent elements. A useful systematic procedure for analyzing a cascaded system

therefore draws on both the wave-transfer and scattering matrix approaches: we use the handy multiplication formula of the **M** matrices and then convert to the **S** matrix to determine the overall transmittance and reflectance of the cascaded system.

EXAMPLE 7.1-1.   *Propagation Through a Homogeneous Medium.*   For a homogeneous layer of width d and refractive index n, the complex amplitudes of the collected waves at the planes indicated by the arrows are related by $U_2^{(+)} = e^{-j\varphi}U_1^{(+)}$ and $U_1^{(-)} = e^{-j\varphi}U_2^{(-)}$, where $\varphi = nk_od$, so that in this case the wave-transfer matrix and the scattering matrix are:

$$\mathbf{M} = \begin{bmatrix} \exp(-j\varphi) & 0 \\ 0 & \exp(j\varphi) \end{bmatrix}, \mathbf{S} = \begin{bmatrix} \exp(-j\varphi) & 0 \\ 0 & \exp(-j\varphi) \end{bmatrix}, \varphi = nk_od.$$

$$(7.1\text{-}4)$$

Relation between Scattering Matrix and Wave-Transfer Matrix

The elements of the **M** and **S** matrices are related by manipulating the defining equations (7.1-1) and (7.1-3), whereupon the following conversion equations emerge:

$$\mathbf{M} = \begin{bmatrix} A & B \\ C & D \end{bmatrix} = \frac{1}{t_{21}} \begin{bmatrix} t_{12}t_{21} - r_{12}r_{21} & r_{21} \\ -r_{12} & 1 \end{bmatrix},$$

$$(7.1\text{-}5)$$

$$\mathbf{S} = \begin{bmatrix} t_{12} & r_{21} \\ r_{12} & t_{21} \end{bmatrix} = \frac{1}{D} \begin{bmatrix} AD - BC & B \\ -C & 1 \end{bmatrix}.$$

$$(7.1\text{-}6)$$
Conversion
Relations

These equations are not valid in the limiting cases when $t_{21} = 0$ or $D = 0$.

Summary

Matrix wave optics offers a systematic procedure for determining the amplitude transmittance and reflectance of a stack of dielectric layers with prescribed thicknesses and refractive indexes:

- The stack is divided into a cascade of elements encompassing boundaries with homogeneous layers between them.

- The **M** matrix is determined for each element. This may be achieved by using the Fresnel formulas for transmission and reflection to determine its **S** matrix, and then using the conversion relation (7.1-5) to calculate the corresponding **M** matrix.

- The **M** matrix for the full stack of elements is obtained by simply multiplying the **M** matrices for the individual elements, in accordance with the wave-transfer matrix formula provided in (7.1-2).

- Finally, the **S** matrix for the full stack is determined by conversion from the overall **M** matrix via (7.1-6). The elements of the **S** matrix then directly yield the amplitude transmittance and reflectance for the full stack of dielectric layers.

Two Cascaded Systems: Airy's Formulas.

Matrix methods may be used to derive explicit expressions for elements of the scattering matrix of a composite system in terms of elements of the scattering matrices of the constituent systems. Consider a wave transmitted through a system described by an **S** matrix with elements t_{12}, r_{21}, r_{12}, and t_{21}, followed by another system with **S** matrix elements t_{23}, r_{32}, r_{23}, and t_{32}. By multiplying the two associated **M** matrices, and then converting the result to an **S** matrix, the following formulas for the overall forward transmittance and reflectance can be derived:

$$t_{13} = \frac{t_{12}t_{23}}{1 - r_{21}r_{23}}, \quad r_{13} = r_{12} + \frac{t_{12}t_{21}r_{23}}{1 - r_{21}r_{23}}. \tag{7.1-7}$$

If the two cascaded systems are mediated by propagation through a homogeneous medium, as illustrated in Fig. 7.1-2, then by use of the wave-transmission matrix in (7.1-4), with the phase $\varphi = nk_o d$, where d is the propagation distance and n is the refractive index of the medium, the following formulas for the overall transmittance and reflectance, known as the **Airy's formulas**, may be derived:

$$t_{13} = \frac{t_{12}t_{23}\exp(-j\varphi)}{1 - r_{21}r_{23}\exp(-j2\varphi)}, \quad r_{13} = r_{12} + \frac{t_{12}t_{21}r_{23}\exp(-j2\varphi)}{1 - r_{21}r_{23}\exp(-j2\varphi)}. \tag{7.1-8}$$
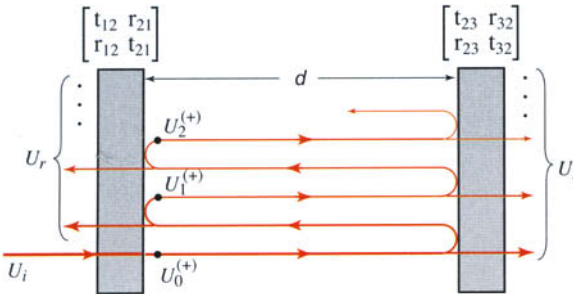
Airy's Formulas

Figure 7.1-2 Transmission of a plane wave through a cascade of two separated systems.

The Airy's formulas may also be derived by tracking the multiple transmissions and reflections undergone by an incident wave between the two systems and adding up their amplitudes, as portrayed in Fig. 7.1-2. A plane wave of complex amplitude U_i incident on the first system produces an initial internal wave of amplitude $U_0^{(+)} = t_{12}U_i$, which reflects back and forth between the two subsystems producing additional internal waves $U_1^{(+)}, U_2^{(+)}, \ldots$, all traveling in the forward direction. The amplitude of the overall transmitted wave U_t is related to the total internal amplitude $U^{(+)} = U_0^{(+)} + U_1^{(+)} + \cdots$ by $U_t = t_{23}\exp(-j\phi)U^{(+)}$, where $\phi = nk_o d$. The overall amplitude transmittance is therefore $t_{13} = U_t/U_i = t_{12}t_{23}\exp(-j\phi)(U^{(+)}/U_0^{(+)})$. Since $U^{(+)} = U_0^{(+)}(1 + h + h^2 + \cdots) = U_0^{(+)}/(1 - h)$, where $h = r_{21}r_{23}\exp(-j2\phi)$ is the round-trip multiplication factor, the overall amplitude transmittance t_{13} yields the Airy's formula in (7.1-8).

Conservation Relations for Lossless Media

If the medium between planes 1 and 2 is nonlossy, then the incoming and outgoing optical powers must be equal. Furthermore, if the media at the input and output planes have the same impedance and refractive index, then these powers are represented by

the squared magnitudes of the complex amplitudes $\left|U_{1,2}^{(\pm)}\right|^2$. In this case, conservation of power dictates that $\left|U_1^{(+)}\right|^2 + \left|U_2^{(-)}\right|^2 = \left|U_2^{(+)}\right|^2 + \left|U_1^{(-)}\right|^2$ for any combination of incoming amplitudes. By choosing the incoming amplitudes $U_1^{(+)}$ and $U_2^{(-)}$ to be (1,0), (0,1), and (1,1), *the conservation formula above yields three equations that relate the* elements of the **S** matrix. These equations can be used to prove the following formulas:

$$|t_{12}| = |t_{21}| \equiv |t|, \quad |r_{12}| = |r_{21}| \equiv |r|, \quad |t|^2 + |r|^2 = 1, \qquad (7.1\text{-}9)$$

$$t_{12}/t_{21}^* = -r_{12}/r_{21}^*. \qquad (7.1\text{-}10)$$

Equations (7.1-9) relate the magnitudes of the elements of the **S** matrix for lossless media whose input and output planes see the same refractive index, whereas (7.1-10) relates their arguments.

The formulas in (7.1-9) and (7.1-10) translate to the following relations among the elements of the **M** matrix:

$$|D| = |A|, \quad |C| = |B|, \quad |A|^2 - |B|^2 = 1, \qquad (7.1\text{-}11)$$

$$\det \mathbf{M} = C/B^* = A/D^* = t_{12}/t_{21}, \quad |\det \mathbf{M}| = 1. \qquad (7.1\text{-}12)$$

These results can be derived by substituting the conservation relations for lossless media, (7.1-9) and (7.1-10), into the conversion relations between the wave-transfer and scattering matrices, (7.1-5) and (7.1-6).

Lossless Reciprocal Systems

For lossless systems with reciprocal symmetry, namely systems whose transmission/reflection in the forward and backward directions are identical, we have $t_{21} = t_{12} \equiv t$ and $r_{21} = r_{12} \equiv r$. In this case, (7.1-9) and (7.1-10) yield

$$|t|^2 + |r|^2 = 1, \quad t/r = -(t/r)^*, \quad \arg\{t\} - \arg\{r\} = \pm\pi/2, \qquad (7.1\text{-}13)$$

indicating that the phases associated with transmission and reflection differ by $\pi/2$. Under these conditions, the elements of the **M** matrix satisfy the following relations:

$$A = D^*, \quad B = C^*, \quad |A|^2 - |B|^2 = 1, \quad \det \mathbf{M} = 1. \qquad (7.1\text{-}14)$$

The **S** and **M** matrices then take the simple form

$$\mathbf{S} = \begin{bmatrix} t & r \\ r & t \end{bmatrix}, \quad \mathbf{M} = \begin{bmatrix} 1/t^* & r/t \\ r^*/t^* & 1/t \end{bmatrix}, \qquad \begin{array}{l} (7.1\text{-}15) \\ \text{Lossless Reciprocal System} \end{array}$$

and the system is described by two complex numbers t and r related by (7.1-13).

EXAMPLE 7.1-2.   *Partially Reflective Mirror (Beamsplitter).* A lossless partially reflective mirror placed in a homogeneous medium is a reciprocal system with an **S** matrix given by (7.1-15). Assuming that the phase $\arg\{t\} = 0$, then (7.1-13) dictates that $\arg\{r\} = \mp\pi/2$, so that $r = \mp j|r|$. Using the $+$ sign, a model for the scattering matrix of the beamsplitter is:

$$\mathbf{S} = \begin{bmatrix} |t| & j|r| \\ j|r| & |t| \end{bmatrix}, \quad |t|^2 + |r|^2 = 1. \qquad (7.1\text{-}16)$$

The corresponding **M** matrix is:
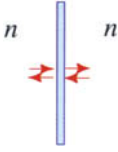
$$\mathbf{M} = \frac{1}{|\mathbf{t}|} \begin{bmatrix} 1 & j|\mathbf{r}| \\ -j|\mathbf{r}| & 1 \end{bmatrix}. \tag{7.1-17}$$

An ideal mirror has an **S** matrix given by (7.1-16) with $|\mathbf{r}| = 1$ and $|\mathbf{t}| = 0$. In this limiting case, (7.1-17) is not applicable and the **M** matrix does not provide an appropriate representation since the two sides of the perfect mirror are isolated and independent.

EXAMPLE 7.1-3. *Single Dielectric Boundary.* In this example, the system comprises a single boundary. In accordance with the Fresnel equations (see Sec. 6.2), the transmittance and reflectance at a boundary between two media of refractive indexes n_1 and n_2 are defined by the **S** matrix

$$\mathbf{S} = \begin{bmatrix} \mathbf{t}_{12} & \mathbf{r}_{21} \\ \mathbf{r}_{12} & \mathbf{t}_{21} \end{bmatrix} = \frac{1}{n_1 + n_2} \begin{bmatrix} 2n_1 & n_2 - n_1 \\ n_1 - n_2 & 2n_2 \end{bmatrix}. \tag{7.1-18}$$

Substitution into (7.1-5) yields the **M** matrix
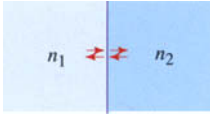
$$\mathbf{M} = \frac{1}{2n_2} \begin{bmatrix} n_2 + n_1 & n_2 - n_1 \\ n_2 - n_1 & n_2 + n_1 \end{bmatrix}. \tag{7.1-19}$$

EXAMPLE 7.1-4. *Propagation Followed by a Boundary.* The **M** matrix of a homogeneous layer of width d followed by a boundary is given by the **M** matrix for the boundary, (7.1-19), multiplied by the **M** matrix for the homogeneous layer, (7.1-4):
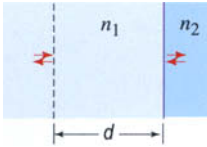
$$\mathbf{M} = \frac{1}{2n_2} \begin{bmatrix} (n_2 + n_1)\, e^{-j\varphi} & (n_2 - n_1)\, e^{j\varphi} \\ (n_2 - n_1)\, e^{-j\varphi} & (n_2 + n_1)\, e^{j\varphi} \end{bmatrix}, \quad \varphi = n_1 k_o d. \tag{7.1-20}$$

EXAMPLE 7.1-5. *Propagation Followed by Transmission Through a Slab.* This system comprises a cascade of two subsystems, both of the type considered in Example 7.1-4. In the first system the light travels from a medium of index n_1 to a medium of index n_2, whereas in the second system the light travels from a medium of index n_2 to a medium of index n_1. By virtue of (7.1-2), the overall **M** matrix is a product of the constituent **M** matrices, with the matrix multiplication taking place in reverse order:
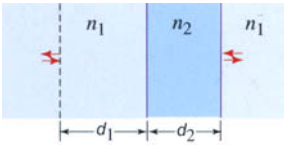
$$\mathbf{M} = \frac{1}{4n_1 n_2} \begin{bmatrix} (n_1 + n_2)\, e^{-j\varphi_2} & (n_1 - n_2)\, e^{j\varphi_2} \\ (n_1 - n_2)\, e^{-j\varphi_2} & (n_1 + n_2)\, e^{j\varphi_2} \end{bmatrix}$$

$$\times \begin{bmatrix} (n_2 + n_1)\, e^{-j\varphi_1} & (n_2 - n_1)\, e^{j\varphi_1} \\ (n_2 - n_1)\, e^{-j\varphi_1} & (n_2 + n_1)\, e^{j\varphi_1} \end{bmatrix}. \tag{7.1-21}$$

Here $\varphi_1 = n_1 k_o d_1$ and $\varphi_2 = n_2 k_o d_2$, where d_1 and d_2 are the widths of the two regions, respectively. Elements of the matrix **M**, which are given by

$$A = D^* = \frac{1}{\mathbf{t}^*} = \frac{1}{4n_1 n_2} \left[(n_1 + n_2)^2\, e^{-j\varphi_2} - (n_2 - n_1)^2\, e^{j\varphi_2} \right] e^{-j\varphi_1}, \tag{7.1-22}$$

$$B = C^* = \frac{\mathbf{r}}{\mathbf{t}} = \frac{1}{4n_1 n_2} (n_2^2 - n_1^2) \left[e^{-j\varphi_2} - e^{j\varphi_2} \right] e^{j\varphi_1}, \tag{7.1-23}$$

satisfy the properties of a reciprocal and lossless system, as described by (7.1-14).

From (7.1-22) and (7.1-23) we can determine expressions for t and r. Thus,

$$\mathsf{t} = \exp(-j\varphi_1)\frac{4n_1 n_2 \exp(-j\varphi_2)}{(n_1 + n_2)^2 - (n_1 - n_2)^2 \exp(-j2\varphi_2)}. \qquad (7.1\text{-}24)$$

This expression can also be directly derived by regarding the system as a combination of two bound-aries mediated by propagation through a distance in a medium, and using the Airy's formula (7.1-8) with $\mathsf{t}_{12} = \mathsf{t}_{32} = 2n_1/(n_1 + n_2)$, $\mathsf{t}_{21} = \mathsf{t}_{23} = 2n_2/(n_1 + n_2)$, $\mathsf{r}_{12} = \mathsf{r}_{32} = -\mathsf{r}_{21} = -\mathsf{r}_{23} = (n_1 - n_2)/(n_1 + n_2)$.

EXERCISE 7.1-1

Quarter-Wave Film as an Anti-Reflection Coating.   Specially designed thin films are often used to reduce or eliminate reflection at the boundary between two media of different refractive indexes. Consider a thin film of refractive index n_2 and thickness d sandwiched between media of refractive indexes n_1 and n_3. Derive an expression for the B element of the $\mathbf{M}$ matrix for this multilayer medium. Show that light incident from medium 1 has zero reflectance if $d = \lambda/4$ and $n_2 = \sqrt{n_1 n_3}$, where $\lambda = \lambda_o/n_2$.
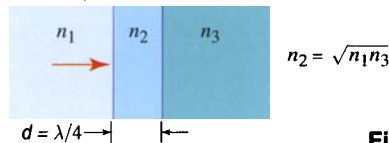

Figure 7.1-3   Anti-reflection coating.

Off-Axis Waves in Layered Media

When an oblique wave is incident on a layered medium, the transmitted and reflected waves, along with their reflections and transmissions in turn, bounce back and forth between the layers, as illustrated by its real part as shown in Fig. 7.1-4(a). The laws of reflection and refraction ensure that, within the same layer, all of the forward waves are parallel, and all of the backward waves are parallel. Moreover, within any given layer the forward and backward waves travel at the same angle, when measured from the $+z$ and $-z$ directions, respectively.

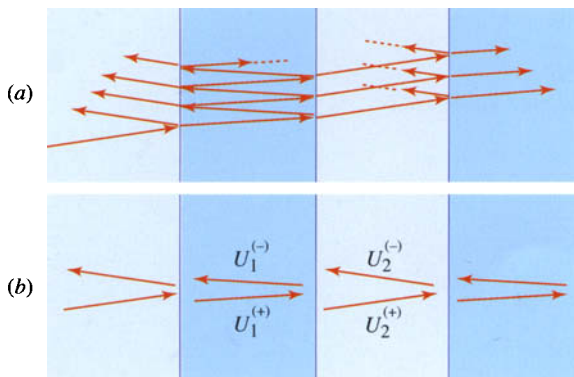**Figure 7.1-4**   (a) Reflections of a single incident oblique wave from the boundaries of a multilayered medium. (b) In each layer, the forward waves are lumped into a collected forward wave, and the backward waves are lumped into a collected backward wave.

The "macro" approach that was used earlier for normally incident waves is similarly applicable for oblique waves. The distinction is that the Fresnel transmittances

and reflectances at a boundary, t_{12}, r_{21}, r_{12}, and t_{21}, are angle-dependent as well as polarization-dependent (see Sec. 6.2).

The simplest example is propagation a distance d through a homogeneous medium of refractive index n, at an angle θ measured from the z axis. The wave-transfer matrix $\mathbf{M}$ is then given by (7.1-4), where the phase is now $\varphi = nk_o d \cos\theta$. Two other examples are presented below.

EXAMPLE 7.1-6. *Single Boundary: Oblique TE Wave.* A wave transmitted through a planar boundary between media of refractive indexes n_1 and n_2 at angles θ_1 and θ_2, satisfying Snell's law ($n_1 \sin\theta_1 = n_2 \sin\theta_2$), is described by an $\mathbf{S}$ matrix determined from the Fresnel equations (6.2-8) and (6.2-9), and its corresponding $\mathbf{M}$ matrix:
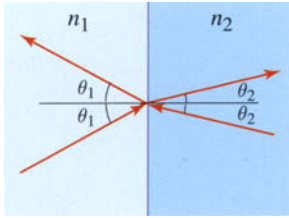
$$\mathbf{S} = \begin{bmatrix} t_{12} & r_{21} \\ r_{12} & t_{21} \end{bmatrix} = \frac{1}{\widetilde{n}_1 + \widetilde{n}_2} \begin{bmatrix} 2a_{12}\widetilde{n}_1 & \widetilde{n}_2 - \widetilde{n}_1 \\ \widetilde{n}_1 - \widetilde{n}_2 & 2a_{21}\widetilde{n}_2 \end{bmatrix}, \qquad (7.1\text{-}25)$$

$$\mathbf{M} = \begin{bmatrix} A & B \\ C & D \end{bmatrix} = \frac{1}{2a_{21}\widetilde{n}_2} \begin{bmatrix} \widetilde{n}_1 + \widetilde{n}_2 & \widetilde{n}_2 - \widetilde{n}_1 \\ \widetilde{n}_2 - \widetilde{n}_1 & \widetilde{n}_1 + \widetilde{n}_2 \end{bmatrix}. \qquad (7.1\text{-}26)$$

These expressions are applicable for both TE and TM polarized waves with the following definitions:

TE: $\quad \widetilde{n}_1 = n_1 \cos\theta_1, \quad \widetilde{n}_2 = n_2 \cos\theta_2, \quad a_{12} = a_{21} = 1,$

TM: $\quad \widetilde{n}_1 = n_1 \sec\theta_1, \quad \widetilde{n}_2 = n_2 \sec\theta_2, \quad a_{12} = \cos\theta_1 / \cos\theta_2 = 1/a_{21}.$

EXAMPLE 7.1-7. *Propagation Followed by Transmission Through a Slab: Off-Axis Wave.* This example deals with an oblique wave traveling through the system described in Example 7.1-5: a slab of thickness d_2 and refractive index n_2 in a medium of refractive index n_1. The wave travels a distance d_1 in the surrounding medium before it crosses into the slab. The wave-transfer matrix for an oblique wave is a generalization of the on-axis result:
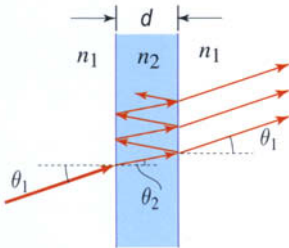
$$\mathbf{M} = \frac{1}{4\widetilde{n}_1 \widetilde{n}_2} \begin{bmatrix} (\widetilde{n}_1 + \widetilde{n}_2)\, e^{-j\widetilde{\varphi}_2} & (\widetilde{n}_1 - \widetilde{n}_2)\, e^{j\widetilde{\varphi}_2} \\ (\widetilde{n}_1 - \widetilde{n}_2)\, e^{-j\widetilde{\varphi}_2} & (\widetilde{n}_1 + \widetilde{n}_2)\, e^{j\widetilde{\varphi}_2} \end{bmatrix}$$

$$\times \begin{bmatrix} (\widetilde{n}_2 + \widetilde{n}_1)\, e^{-j\widetilde{\varphi}_1} & (\widetilde{n}_2 - \widetilde{n}_1)\, e^{j\widetilde{\varphi}_1} \\ (\widetilde{n}_2 - \widetilde{n}_1)\, e^{-j\widetilde{\varphi}_1} & (\widetilde{n}_2 + \widetilde{n}_1)\, e^{j\widetilde{\varphi}_1} \end{bmatrix}, \qquad (7.1\text{-}27)$$

where $\widetilde{\varphi}_1 = n_1 k_o d_1 \cos\theta_1$ and $\widetilde{\varphi}_2 = n_2 k_o d_2 \cos\theta_2$, and, as in Example 7.1-6, $\widetilde{n}_1 = n_1 \cos\theta_1$ and $\widetilde{n}_2 = n_2 \cos\theta_2$ for the TE polarization, and $\widetilde{n}_1 = n_1 \sec\theta_1$ and $\widetilde{n}_2 = n_2 \sec\theta_2$ for the TM polarization.

The expression for the matrix $\mathbf{M}$ in (7.1-27) is identical to that provided in (7.1-21), which describes the on-axis system, except that the parameters n_1, n_2, φ_1, and φ_2 are replaced by the angle- and polarization-dependent parameters $\widetilde{n}_1$ and $\widetilde{n}_2$, and by the angle-dependent parameters $\widetilde{\varphi}_1$ and $\widetilde{\varphi}_2$. Note that the factors a_{12} and a_{21}, which appear in (7.1-26) at each boundary, cancel out since $a_{12}a_{21} = 1$: With these substitutions, the expression (7.1-24) for the on-axis transmittance developed in Example 7.1-5 is generalized to the off-axis, polarization-dependent case,

$$t = \exp(-j\widetilde{\varphi}_1) \frac{4\widetilde{n}_1 \widetilde{n}_2 \exp(-j\widetilde{\varphi}_2)}{(\widetilde{n}_1 + \widetilde{n}_2)^2 - (\widetilde{n}_1 - \widetilde{n}_2)^2 \exp(-j2\widetilde{\varphi}_2)}. \qquad (7.1\text{-}28)$$

B. Fabry–Perot Etalon

The Fabry–Perot etalon was introduced in Sec. 2.5B as an interferometer made of two parallel highly reflective mirrors that transmit light only at a set of specific uniformly spaced frequencies, which depend on the optical pathlength between the mirrors. It is used both as a filter and as a spectrum analyzer, and is controlled by varying the pathlength, e.g., by moving one of the mirrors. It is also used as an optical resonator, as discussed in Sec. 10.1. In this section, we examine this multilayer device using the matrix methods developed in this chapter.

Mirror Fabry–Perot Etalon

Consider two lossless partially reflective mirrors with amplitude transmittances t_1 and t_2, and amplitude reflectances r_1 and r_2, separated by a distance d filled with a medium of refractive index n. The overall system is described by the matrix product

$$\mathbf{M} = \begin{bmatrix} 1/t_1^* & r_1/t_1 \\ r_1^*/t_1^* & 1/t_1 \end{bmatrix} \begin{bmatrix} \exp(-j\varphi) & 0 \\ 0 & \exp(j\varphi) \end{bmatrix} \begin{bmatrix} 1/t_2^* & r_2/t_2 \\ r_2^*/t_2^* & 1/t_2 \end{bmatrix}, \qquad (7.1\text{-}29)$$

where $\varphi = nk_o d$. Since the system is lossless and reciprocal, $\mathbf{M}$ takes the simplified form provided in (7.1-15) and the amplitude transmittance t is therefore the inverse of the D element of $\mathbf{M}$, so that

$$t = \frac{t_1 t_2 \exp(-j\varphi)}{1 - r_1 r_2 \exp(-j2\varphi)}. \qquad (7.1\text{-}30)$$

This relation may also be derived by direct use of the Airy's formula (7.1-8).

As a result, the intensity transmittance of the etalon is

$$\mathcal{T} = |t|^2 = \frac{|t_1 t_2|^2}{|1 - r_1 r_2 \exp(-j2\varphi)|^2}. \qquad (7.1\text{-}31)$$

This expression is similar to (2.5-16) for the intensity of an infinite number of waves with equal phase differences, and with amplitudes that decrease at a geometric rate, as described in Sec.2.5B. Assuming that $\arg\{r_1 r_2\} = 0$, this expression can be written in the form[†]

$$\mathcal{T} = \frac{\mathcal{T}_{\max}}{1 + (2\mathcal{F}/\pi)^2 \sin^2 \varphi}, \qquad (7.1\text{-}32)$$

where

$$\mathcal{T}_{\max} = \frac{|t_1 t_2|^2}{(1 - |r_1 r_2|)^2} = \frac{(1 - |r_1|^2)(1 - |r_2|^2)}{(1 - |r_1 r_2|)^2} \qquad (7.1\text{-}33)$$

and

$$\boxed{\mathcal{F} = \frac{\pi \sqrt{|r_1 r_2|}}{1 - |r_1 r_2|}.} \qquad (7.1\text{-}34)$$

Finesse

[†] This expression reproduces (2.5-18) if φ is replaced by the round-trip phase 2φ.

The parameter $\mathcal{F}$, called the **finesse**, is a monotonic increasing function of the reflectance product $r_1 r_2$, and is a measure of the quality of the etalon. For example, if $r_1 r_2 = 0.99$, then $\mathcal{F} \approx 313$.

As described in Sec. 2.5B, the transmittance $\mathcal{T}$ is a periodic function of φ with period π. It reaches its maximum value of $\mathcal{T}_{\max}$, which equals unity if $|r_1| = |r_2|$, when φ is an integer multiple of π. When the finesse $\mathcal{F}$ is large (i.e., when $|r_1 r_2| \approx 1$), $\mathcal{T}$ becomes a sharply peaked function of φ of approximate width $\pi/\mathcal{F}$. Thus, the higher the finesse $\mathcal{F}$, the sharper the peaks of the transmittance as a function of the phase φ.

The phase $\varphi = n k_o d = (\omega/c)d$ is proportional to the frequency, so that the condition $\varphi = \pi$ corresponds to $\omega = \omega_F$, or $\nu = \nu_F$, where

$$\nu_F = \frac{c}{2d}, \qquad \omega_F = \frac{\pi c}{d}$$

(7.1-35)
Free Spectral Range

is called the **free spectral range**. It follows that the transmittance as a function of frequency, $\mathcal{T}(\nu)$, is a periodic function of period ν_F,

$$\mathcal{T}(\nu) = \frac{\mathcal{T}_{\max}}{1 + (2\mathcal{F}/\pi)^2 \sin^2(\pi\nu/\nu_F)},$$

(7.1-36)
Transmittance
(Fabry–Perot Etalon)

as illustrated in Fig. 7.1-5. It reaches its peak value of $\mathcal{T}_{\max}$ at the resonance frequencies $\nu_q = q\nu_F$, where q is an integer. When the finesse $\mathcal{F} \gg 1$, $\mathcal{T}(\nu)$ drops sharply as the frequency deviates slightly from ν_q, so that $\mathcal{T}(\nu)$ takes the form of a comb-like function. The spectral width of each of these high-transmittance lines is

$$\delta\nu = \frac{\nu_F}{\mathcal{F}},$$

(7.1-37)

i.e., is a factor of $\mathcal{F}$ smaller than the spacing between the resonance frequencies.
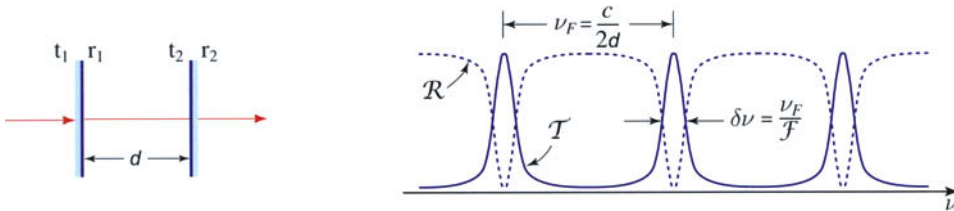

Figure 7.1-5 Intensity transmittance and reflectance, $\mathcal{T}$ and $\mathcal{R} = 1 - \mathcal{T}$, of the Fabry–Perot etalon as a function of the angular frequency ω.

The Fabry–Perot etalon may be used as a sharply tuned optical filter or a spectrum analyzer. Because of the periodic nature of the spectral response, however, the spectral width of the measured light must be narrower than the free spectral range $\nu_F = c/2d$ in order to avoid ambiguity. The filter is tuned (i.e., the resonance frequencies are shifted) by adjusting the distance d between the mirrors. A slight change in mirror spacing Δd shifts the resonance frequency $\nu_q = qc/2d$ by a relatively large amount $\Delta\nu_q = -(qc/2d^2)\Delta d = -\nu_q \Delta d/d$. Although the frequency spacing ν_F

also changes, it is by the far smaller amount $-\nu_F \Delta d / d$. As an example, a mirror separation $d = 1.5$ cm leads to a free spectral range $\nu_F = 10$ GHz when $n = 1$. For a typical optical frequency of $\nu = 10^{14}$ Hz, corresponding to $q = 10^4$, a change of d by a factor of 10^{-4} ($\Delta d = 1.5~\mu$m) translates the peak frequency by $\Delta \nu_q = 10$ GHz, whereas the free spectral range is altered by only 1 MHz, becoming 9.999 GHz.

Applications of the Fabry–Perot etalon as a resonator are described in Sec. 10.1.

The Dielectric-Slab as a Fabry–Perot Etalon

Based on (7.1-24), the transmittance of a dielectric slab of width d and refractive index n_2 in a medium of refractive index n_1 is

$$t = \frac{4n_1 n_2 \exp(-j\varphi)}{(n_1 + n_2)^2 - (n_1 - n_2)^2 \exp(-j2\varphi)}, \qquad (7.1-38)$$

where $\varphi = n_2 k_o d$. This expression reproduces (7.1-30), which applies to the Fabry–Perot etalon, if we substitute $t_1 t_2 = 4n_1 n_2 / (n_1 + n_2)$ and $r_1 r_2 = (n_1 - n_2)^2 / (n_1 + n_2)^2$. It follows that the expressions for the intensity transmittance of the mirror etalon, (7.1-32) and (7.1-36), are applicable to the dielectric slab. Using (7.1-34), the finesse of the slab is given by

$$\mathcal{F} = \frac{\pi}{4} \frac{|n_2^2 - n_1^2|}{n_1 n_2}. \qquad (7.1-39)$$

Large values of $\mathcal{F}$ are not normally obtained in slab etalons. For example, for $n_1 = 1.5$ (the refractive index of SiO_2) and $n_2 = 3.5$ (the refractive index of Si), $\mathcal{F} = 1.68$. As illustrated in Fig. 7.1-6, the frequency dependence of $\mathcal{T}$ in this case does not exhibit the sharp peaks seen in etalons with highly reflective mirrors, as displayed in Fig. 7.1-5. To obtain higher values of $\mathcal{F}$ the surfaces of the slab must be coated to enhance internal reflection.
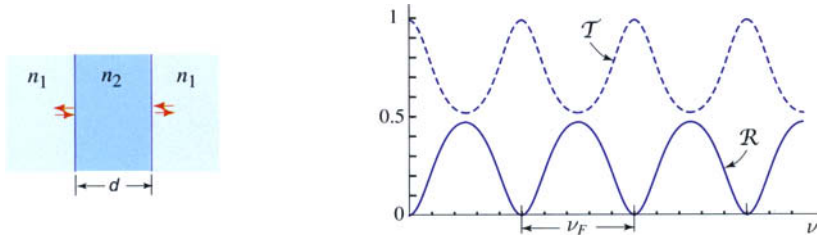

Figure 7.1-6   Frequency dependence of the intensity transmittance and reflectance, $\mathcal{T}$ and $\mathcal{R}$, respectively, of a slab with refractive index $n_2 = 3.5$ (the refractive index of Si) in a medium with refractive index $n_1 = 1.5$ (the refractive index of SiO_2).

Off-Axis Transmittance of the Fabry–Perot Etalon

For an oblique wave traveling at an angle θ with the axis of a mirror etalon, the amplitude transmittance is given by (7.1-30) with the phase φ replaced by $\widetilde{\varphi} = n k_o d \cos \theta$. It follows that the intensity transmittance in (7.1-36) is generalized to

$$\mathcal{T}(\nu) = \frac{\mathcal{T}_{\max}}{1 + (2\mathcal{F}/\pi)^2 \sin^2(\pi \cos \theta \, \nu / \nu_F)}, \qquad (7.1-40)$$

in the off-axis case.

Maximum transmittance occurs at frequencies for which

$$\nu = q\,\nu_F \sec\theta\,,\qquad q = 1, 2, \ldots, \quad \nu_F = c/2d.\qquad (7.1\text{-}41)$$

Resonance
Condition

If the finesse of the etalon is large, transmission occurs at these frequencies and is almost completely blocked at all other frequencies. The plot of this relation provided in Fig. 7.1-7(c) shows that at each angle θ only a set of discrete frequencies are transmitted. Likewise, a wave at frequency ν is transmitted at only a set of angles, so that a cone of incident broad-spectrum (white) light creates a set of concentric rings spread like a rainbow, as illustrated in Fig. 7.1-7(b). For incident light with a spectral width smaller than the free spectral range ν_F, each frequency component corresponds to one and only one angle, so that the etalon can be used as a spectrum analyzer.
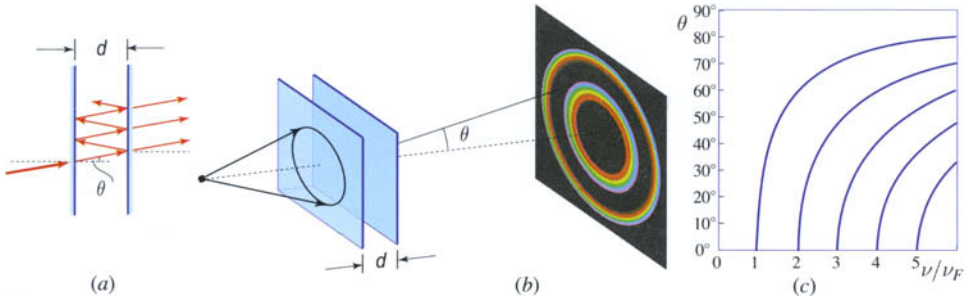

Figure 7.1-7 (a) An off-axis wave transmitted through a mirror Fabry–Perot etalon. (b) White light from a point source transmitted through the etalon creates a set of concentric rings of different frequencies (colors). (c) Frequencies and angles that satisfy the condition of peak transmittance, as set forth in (7.1-41).

C. Bragg Grating

The Bragg grating was introduced in Exercise 2.5-3 as a set of uniformly spaced parallel partially reflective planar mirrors. Such a structure has angular and frequency selectivity that is useful in many applications. In this section, we generalize the definition of the Bragg grating to include a set of N uniformly spaced identical multilayer segments, and develop a theory for light reflection based on matrix wave optics.

Simplified Theory

The reflectance of the Bragg grating was determined in Exercise 2.5-3 under two assumptions: (1) the mirrors are weakly reflective so that the incident wave is not depleted as it propagates, and (2) secondary reflections (i.e., reflections of the reflected waves) are negligible. In this approximation, the reflectance $\mathcal{R}_N$ of an N-mirror grating is related to the reflectance R of a single mirror by the relation[†]

$$\mathcal{R}_N = \frac{\sin^2 N\varphi}{\sin^2 \varphi}\, R.\qquad (7.1\text{-}42)$$

[†] Note that in Exercise 2.5-3 φ denotes the phase between successive phasors, while here that phase is denoted 2φ since it represents a round-trip phase.

As described in Sec. 2.5B, the factor $\sin^2 N\varphi / \sin^2 \varphi$ represents the intensity of the sum of N phasors of unit amplitude and phase difference 2φ. This function has a peak value of N^2 when the Bragg condition is satisfied, i.e., when 2φ equals $q2\pi$, where $q = 0, 1, 2, \ldots$. It drops away from these values sharply, with a width that is inversely proportional to N. In this simplified model, the intensity of the total reflected wave is, at most, a factor of N^2 greater than the intensity of the wave reflected from a single segment.

For a Bragg grating comprising partially reflective mirrors separated from each other by a distance Λ and a round-trip phase $2\varphi = 2k\Lambda \cos\theta$, where θ is the angle of incidence. Therefore, maximum reflection occurs when $2k\Lambda \cos\theta = 2q\pi$ or

$$\cos\theta = q\frac{\lambda}{2\Lambda} = q\frac{\omega_\mathcal{B}}{\omega} = q\frac{\nu_\mathcal{B}}{\nu},$$

(7.1-43)
Bragg Condition

where

$$\nu_\mathcal{B} = \frac{c}{2\Lambda}, \qquad \omega_\mathcal{B} = \frac{\pi c}{\Lambda},$$

(7.1-44)
Bragg Frequency

is the Bragg frequency.
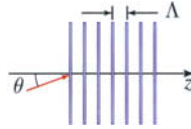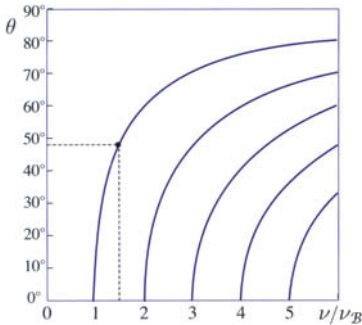
Figure 7.1-8   Locus of frequencies ν and angles θ at which the Bragg condition is satisfied. For example, if $\nu = 1.5\,\nu_\mathcal{B}$, then $\theta = 48.2°$. This corresponds to a Bragg angle $\theta_\mathcal{B} = 41.8°$ (measured from the plane of the grating.)

At normal incidence ($\theta = 0°$), peak reflectance occurs at frequencies that are integer multiples of the Bragg frequency, i.e., $\nu = q\nu_\mathcal{B}$. At frequencies such that $\nu < \nu_\mathcal{B}$, the Bragg condition cannot be satisfied at any angle. At frequencies $\nu_\mathcal{B} < \nu < 2\nu_\mathcal{B}$, the Bragg condition is satisfied at one angle $\theta = \cos^{-1}(\lambda/2\Lambda) = \cos^{-1}(\nu_\mathcal{B}/\nu)$. The complement of this angle, $\theta_\mathcal{B} = \pi/2 - \theta$, is the Bragg angle (see (2.5-13) and Fig. 2.5-8),

$$\theta_\mathcal{B} = \sin^{-1}(\lambda/2\Lambda).$$

(7.1-45)
Bragg Angle

At frequencies $\nu \geq 2\nu_\mathcal{B}$, the Bragg condition is satisfied at more than one angle. Figure 7.1-8 illustrates the spectral and angular dependence of reflections from a Bragg grating, based on the simplified theory.

Matrix Theory

We now use the matrix approach introduced in the previous section to develop an exact theory of Bragg reflection that includes multiple transmissions and reflections, as well as depletion of the incident wave. It turns out that the collaborative effects of the reflections, and the reflections of reflections, can lead to enhancement of the total reflected wave, and a phenomenon whereby total reflection occurs not only at single frequencies that are multiples of $\nu_B / \cos \theta$, but over extended spectral bands surrounding these frequencies!

Consider a grating comprising a stack of N identical generic segments (Fig. 7.1-9), each described by a unimodular wave-transfer matrix $\mathbf{M}_o$ satisfying the conservation relations for a lossless, reciprocal system, so that

$$\mathbf{M}_o = \begin{bmatrix} 1/t^* & r/t \\ r^*/t^* & 1/t \end{bmatrix}, \tag{7.1-46}$$

where t and r are complex amplitude transmittance and reflectance satisfying the conditions set forth in (7.1-13), and $\mathcal{T} = |t|^2$ and $\mathcal{R} = |r|^2$ are the corresponding intensity transmittance and reflectance.
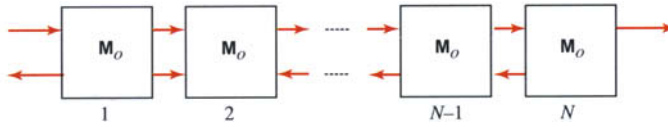

Figure 7.1-9 Bragg grating made of N segments, each of which is described by a matrix $\mathbf{M}_o$.

In accordance with (7.1-2), the wave-transfer matrix $\mathbf{M}$ for the N segments is simply the product $\mathbf{M} = \mathbf{M}_o^N$. Since $\mathbf{M}_o$ is unimodular, i.e., $\det \mathbf{M}_o = 1$, it satisfies the property

$$\mathbf{M}_o^N = \Psi_N \mathbf{M}_o - \Psi_{N-1} \mathbf{I}, \tag{7.1-47}$$

where

$$\Psi_N = \frac{\sin N\Phi}{\sin \Phi}, \tag{7.1-48}$$

$$\cos \Phi = \mathrm{Re}\{1/t\}, \tag{7.1-49}$$

and $\mathbf{I}$ is the identity matrix. Equation (7.1-47) may be proved by induction (i.e., show that this relation is valid for N segments if it is valid for $N - 1$ segments; this may be done by direct substitution and use of trigonometric identities).

Since the N-segment system is also lossless and reciprocal, its matrix may be written in the form

$$\mathbf{M}_o^N = \begin{bmatrix} 1/t_N^* & r_N/t_N \\ r_N^*/t_N^* & 1/t_N \end{bmatrix}, \tag{7.1-50}$$

where t_N and r_N are the N-segment amplitude transmittance and reflectance, respectively. Substituting from (7.1-46) and (7.1-50) into (7.1-47), and comparing the diagonal and off-diagonal elements of the matrices on both sides of the equation, leads to

$$\frac{1}{t_N} = \Psi_N \frac{1}{t} - \Psi_{N-1} \qquad (7.1\text{-}51)$$

$$\frac{r_N}{t_N} = \Psi_N \frac{r}{t}. \qquad (7.1\text{-}52)$$

These two equations define t_N and r_N in terms of t and r.

The intensity transmittance $\mathcal{T}_N = |t_N|^2$ is obtained by taking the absolute-squared value of (7.1-52) and using the relation $\mathcal{R} = 1 - \mathcal{T}$,

$$\mathcal{T}_N = \frac{\mathcal{T}}{\mathcal{T} + \Psi_N^2 (1 - \mathcal{T})}. \qquad (7.1\text{-}53)$$

It follows that the intensity reflectance $\mathcal{R}_N = 1 - \mathcal{T}_N$ is given by

$$\boxed{\mathcal{R}_N = \frac{\Psi_N^2 \mathcal{R}}{1 - \mathcal{R} + \Psi_N^2 \mathcal{R}}.} \qquad (7.1\text{-}54)$$
Bragg-Grating
Reflectance

Summary

The reflectance $\mathcal{R}_N$ of a medium made of N identical segments is related to the single-segment reflectance $\mathcal{R}$ by a nonlinear relation, (7.1-54), which contains a factor Ψ_N resulting from the interference effects associated with collective reflections from the N segments of the grating. Defined by (7.1-48), Ψ_N depends on the number of segments N and another parameter Φ, which is related to the single-segment complex amplitude transmittance t by (7.1-49).

The dependence of $\mathcal{R}_N$ on $\mathcal{R}$, described by (7.1-54), takes simpler forms in certain limits. If the single-segment reflectance is very small, i.e., $\mathcal{R} \ll 1$, and if Ψ_N^2 is not too large so that $\Psi_N^2 \mathcal{R} \ll 1$, then (7.1-54) may be approximated by:

$$\mathcal{R}_N \approx \Psi_N^2 \mathcal{R} = \frac{\sin^2 N\Phi}{\sin^2 \Phi} \mathcal{R}. \qquad (7.1\text{-}55)$$

This relation is now similar in form to the approximate relation (7.1-42), with Φ playing the role of the phase φ.

In the opposite limit for which $\Psi_N^2 \gg 1$, the reflectance $\mathcal{R}_N \approx \Psi_N^2 \mathcal{R}/(1 + \Psi_N^2 \mathcal{R})$. This nonlinear relation between $\mathcal{R}_N$ and $\mathcal{R}$ exhibits saturation and is typical of systems with feedback, which in this case results from multiple internal reflections at the segment boundaries. Ultimately, if $\Psi_N^2 \mathcal{R} \gg 1$, then $\mathcal{R}_N$ approaches its maximum value of unity, so that the N-segment device acts as perfect mirror even though the single segment is only partially reflective. A large interference factor Ψ_N accelerates the rise of $\mathcal{R}_N$ to unity as $\mathcal{R}$ increases.

The interference factor Ψ_N, which depends on $\Phi = \cos^{-1}(\mathrm{Re}\{1/t\})$ via (7.1-48), follows two distinct regimes: i) a normal regime for which Φ is real and the grating exhibits partial reflection/transmission (including zero reflection, or total transmission),

and ii) an anomalous regime for which Φ is complex and Ψ_N can be extremely large, corresponding to total reflection.

Partial- and Zero-Reflection Regime

This regime is defined by the condition $|\text{Re}\{1/t\}| \leqslant 1$, which ensures that $\Phi = \cos^{-1}(\text{Re}\{1/t\})$ is real. In this case, $\mathcal{R}_N$ depends on $\mathcal{R}$ and Ψ_N in accordance with (7.1-48) and (7.1-54). Maximum reflectance occurs when Ψ_N has its maximum value of N. In this case, $\mathcal{R}_N = N^2\mathcal{R}/(1 - \mathcal{R} + N^2\mathcal{R})$. Therefore, $\mathcal{R}_N$ cannot exactly equal unity unless $\mathcal{R} = 1$, exactly. For example, for $N = 10$, if $\mathcal{R} = 0.5$, then the maximum value of $\mathcal{R}_N = \approx 0.99$.

Zero reflectance, or **total transmittance**, is possible, even if the reflectance R of the individual segment is substantial. This occurs when $\Psi_N = 0$, i.e., when $\sin N\Phi = 0$, or $\Phi = q\pi/N$ for $q = 0, 1, \ldots, N-1$. The N frequencies at which this complete transparency occurs are resonance frequencies of the grating. The phenomenon represents some form of tunneling through the individually reflective segments.

Total-Reflection Regime

In this regime, $|\text{Re}\{1/t\}| = |\cos\Phi| > 1$ so that Φ is a complex variable $\Phi = \Phi_R + j\Phi_I$. Using the identity $\cos(\Phi_R + j\Phi_I) = \cos\Phi_R \cosh\Phi_I - j\sin\Phi_R \sinh\Phi_I$, and equating the real and imaginary parts of both sides of (7.1-49), we obtain $\sin\Phi_R = 0$ so that $\Phi_R = m\pi$ and $\cos\Phi_R = +1$, or -1, when m is an even or odd integer, respectively, which results in

$$\cosh\Phi_I = |\text{Re}\{1/t\}|.$$

(7.1-56)
Total-Reflection Regime

The factor $\Psi_N = \sin N\Phi/\sin\Phi$ then becomes

$$\Psi_N = \pm\frac{\sinh N\Phi_I}{\sinh\Phi_I},$$

(7.1-57)
Total-Reflection Regime

where the $\pm$ sign is the sign of the factor $\cos(Nm\pi)/\cos(m\pi)$. Since $\sinh(\cdot)$ increases exponentially with N for large N, $|\Psi_N|$ can be much greater than N. In this case, in accordance with (7.1-54), the reflectance $\mathcal{R}_N \approx 1$ and the grating acts as a total reflector. The forward waves become evanescent and do not penetrate the multisegment medium, much as occurs with total internal reflection.

Because Φ depends on t, which depends on the frequency ν, the two regimes correspond to distinct spectral bands, as illustrated in the following examples. The spectral bands associated with the total-reflection regime are called **stop bands** since they represent bands within which light transmission is almost completely blocked. The other regime corresponds to **passbands**. Total transmission (zero reflection) occurs at specific resonance frequencies within the passbands.

EXAMPLE 7.1-8. *Stack of Partially Reflective Mirrors.* Consider a grating made of a stack of N identical partially reflective mirrors (beamsplitters) that are mutually separated by a distance Λ and embedded in a homogeneous medium of refractive index n, as illustrated in Fig. 7.1-10(a). A single segment comprises a distance Λ in a homogeneous medium, followed by a partially reflective mirror of amplitude transmittance t and amplitude reflectance r.

The wave-transfer matrix $\mathbf{M}_o$ for this segment is determined by multiplying the matrix in (7.1-17) by the matrix in (7.1-4):

$$\mathbf{M}_o = \frac{1}{|t|} \begin{bmatrix} e^{-j\varphi} & j|r|e^{j\varphi} \\ -j|r|e^{-j\varphi} & e^{j\varphi} \end{bmatrix}, \quad \varphi = nk_o\Lambda = \pi\nu/\nu_{\mathcal{B}}, \tag{7.1-58}$$

where $\nu_{\mathcal{B}} = c/2\Lambda$ is the Bragg frequency. This provides $t = |t|e^{j\varphi}$, and therefore Φ via

$$\cos\Phi = \frac{1}{|t|}\cos\varphi \quad \text{for} \quad |\cos\varphi| \le |t|, \tag{7.1-59}$$

$$\cosh\Phi_I = \frac{1}{|t|}|\cos\varphi| \quad \text{for} \quad |\cos\varphi| > |t|. \tag{7.1-60}$$

The relationships between Φ and φ, and between Φ_I and φ, are nonlinear and unusual, as illustrated in Fig. 7.1-10(*b*). The corresponding dependence of the intensity reflectance $\mathcal{R}_N$ on φ is shown in Fig. 7.1-10(*c*). In the normal regime (indicated by the shaded regions), Φ is real and the reflectance exhibits multiple peaks with zeros between. None of the peaks approaches unity, despite the fact that Ψ_N reaches a maximum value of $N = 10$.

The situation is quite different in the total-reflection regime (unshaded regions), where Φ is complex. The factor Ψ_N reaches a value ≈ 3000 at the center of the band ($\varphi = \pi$) when $|t|^2 = 0.5$. These regions represent ranges of φ where total reflection occurs ($\mathcal{R}_N \approx 1$). Since φ is proportional to the frequency ν, Fig. 7.1-10(*c*) is actually a display of the spectral reflectance, and the unshaded regions correspond to the stop bands.
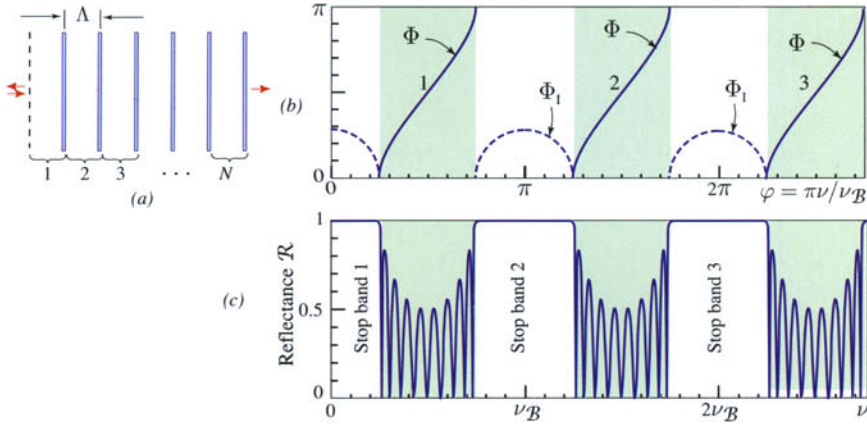

Figure 7.1-10 (*a*) Bragg grating made of $N = 10$ identical mirrors, each with an intensity reflectance $|r|^2 = 0.5$. (*b*) Dependence of Φ on the inter-mirror phase delay $\varphi = nk_o\Lambda$. Within the shaded regions, Φ is complex and its imaginary part Φ_I is represented by the dashed curves. (*c*) Reflectance $\mathcal{R}$ as a function of frequency (in units of the Bragg frequency $\nu_{\mathcal{B}} = c/2\Lambda$). Within the stop bands, the reflectance is approximately unity.

EXAMPLE 7.1-9. *Dielectric Bragg Grating.* A grating is made of N identical dielectric layers of refractive index n_2, each of width d_2, buried in a medium of refractive index n_1 and separated by a distance d_1, as illustrated in Fig. 7.1-11. This multisegment system is a stack of N identical double layers, each of the type described in Example 7.1-5. The $A = 1/t^*$ element of the wave-transfer matrix $\mathbf{M}_o$ is given by (7.1-22), from which

$$\text{Re}\left\{\frac{1}{t}\right\} = \frac{(n_1 + n_2)^2}{4n_1 n_2}\cos(\varphi_1 + \varphi_2) - \frac{(n_2 - n_1)^2}{4n_1 n_2}\cos(\varphi_1 - \varphi_2), \tag{7.1-61}$$

where $\varphi_1 = n_1 k_o d_1$ and $\varphi_2 = n_2 k_o d_2$ are the phases introduced by the two layers of a segment. This result can be used in conjunction with (7.1-48), (7.1-49), (7.1-54), (7.1-56), and (7.1-57) to determine the reflectance of the grating.

The spectral dependence of the reflectance can be computed as a function of ν by noting that $\varphi_1 + \varphi_2 = k_o(n_1 d_1 + n_2 d_2) = \pi\nu/\nu_{\mathcal{B}}$, where $\nu_{\mathcal{B}} = (c_o/\bar{n})/2\Lambda$, and $\bar{n} = (n_1 d_1 + n_2 d_2)/\Lambda$ is

the average refractive index. The Bragg frequency ν_B is the frequency at which the single-segment round-trip phase $2k_o(n_1 d_1 + n_2 d_2) = 2\pi$. The phase difference $\varphi_1 - \varphi_2 = \zeta \pi \nu / \nu_B$, with $\zeta = (n_1 d_1 - n_2 d_2)/(n_1 d_1 + n_2 d_2)$, is also proportional to the frequency. Figure 7.1-11(b) provides an example of the spectral reflectance as a function of ν.
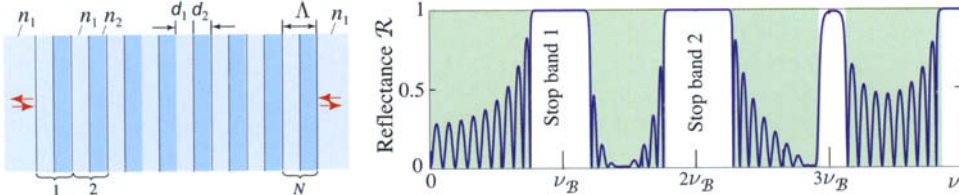

Figure 7.1-11   Intensity reflectance as a function of frequency for a dielectric Bragg grating made of $N = 10$ segments, each of which has two layers of thickness $d_1 = d_2$ and refractive indexes $n_1 = 1.5$ and $n_2 = 3.5$. The grating is placed in a medium with matching refractive index n_1. The reflectance is approximately unity within the shaded stop bands centered about multiples of $\nu_B = c/2\Lambda$, where $c = c_o/\bar{n}$ and $\bar{n}$ is the mean refractive index.

EXAMPLE 7.1-10.   *Dielectric Bragg Grating: Oblique Incidence.*   The results in Example 7.1-9 may be generalized to oblique waves with angle of incidence θ_1 in medium 1, corresponding to angle θ_2 in layer 2, where $n_1 \sin \theta_1 = n_2 \sin \theta_2$. In this case, (7.1-61) becomes

$$\text{Re}\left\{\frac{1}{t}\right\} = \frac{(\tilde{n}_1 + \tilde{n}_2)^2}{4\tilde{n}_1 \tilde{n}_2} \cos(\tilde{\varphi}_1 + \tilde{\varphi}_2) - \frac{(\tilde{n}_2 - \tilde{n}_1)^2}{4\tilde{n}_1 \tilde{n}_2} \cos(\tilde{\varphi}_1 - \tilde{\varphi}_2), \tag{7.1-62}$$

where $\tilde{\varphi}_1 = n_1 k_o d_1 \cos \theta_1$ and $\tilde{\varphi}_2 = n_2 k_o d_2 \cos \theta_2$; $\tilde{n}_1 = n_1 \cos \theta_1$ and $\tilde{n}_2 = n_2 \cos \theta_2$ for TE polarization; and $\tilde{n}_1 = n_1 \sec \theta_1$ and $\tilde{n}_2 = n_2 \sec \theta_2$ for TM polarization. This relation may be used to compute the spectral reflectance at any angle of incidence. Figure 7.1-12 illustrates the dependence of the intensity reflectance R_N on frequency and the angle of incidence for both TE and TM polarization for a high- contrast grating. The range of angles over which unity reflectance obtains increases with increasing refractive-index contrast ratio n_2/n_1.
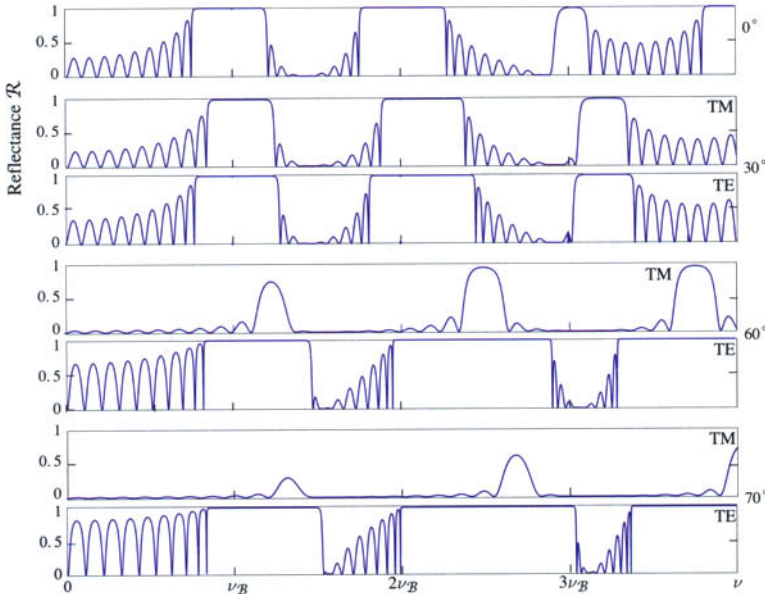

Figure 7.1-12   Spectral dependence of the reflectance $\mathcal{R}$ for the 10-segment dielectric Bragg grating shown in Fig. 7.1-11 at several angles of incidence θ_1 and for TE and TM polarization.

Bragg Grating in an Unmatched Medium

In the previous analysis, the Bragg grating was assumed to be made of N identical segments. If each segment is made of multiple dielectric layers, this requires that grating be placed in a matched medium, i.e., a medium with a refractive index equal to that of the front layer, so that the incident light undergoes no additional reflection at the front boundary, and reflects at the back boundary as if it were entering another layer of the grating. The device described in Example 7.1-9 meets this condition.

In most applications, the grating is placed in an unmatched medium, such as air, and boundary effects must be accounted for. This may be accomplished by writing the wave-transfer matrix **M** of the composite system, including all boundaries, and finding the corresponding scattering matrix **S** by use of the conversion relation. The reflectance of the composite system may be readily determined from **S**.

If $\mathbf{M}_o^N$ is the wave-transfer matrix of an N-segment grating in a medium matched to the front layer, then the overall wave transfer function takes the form

$$\mathbf{M} = \mathbf{M}_e \mathbf{M}_o^{N-1} \mathbf{M}_i, \qquad (7.1\text{-}63)$$

where $\mathbf{M}_i$ is the wave-transfer matrix of the entrance boundary, and $\mathbf{M}_e$ is the wave-transfer matrix of the Nth segment with a boundary into the unmatched medium.

EXAMPLE 7.1-11.   *Reflectance of a Dielectric Bragg Grating in an Unmatched Medium.* An N-segment Bragg grating is made of alternating layers of refractive indexes n_1 and n_2, and widths d_1 and d_2, placed in a medium of refractive index n_0. We wish to determine the reflectance for a wave incident at an angle θ_0 in the external medium, corresponding to angles θ_1 and θ_2 in the first and second layer of each segment, as determined by Snell's law ($n_1 \sin\theta_1 = n_2 \sin\theta_2$).

In this case, (7.1-63) may be used with the following wave-transfer matrices: (1) $\mathbf{M}_i$ represents a boundary between media of refractive indexes n_0 and n_1, as described in Example 7.1-6; (2) $\mathbf{M}_o$ represents a single segment of the grating, as described in Example 7.1-7; (3) $\mathbf{M}_e$ represents propagation a distance d_1 in a medium with refractive index n_1 followed by a slab of width d_2 and refractive index n_2, with boundary into a medium of refractive index n_0. Once the **M** matrix is determined, we use the conversion relation (7.1-6) to determine the corresponding scattering matrix **S**. The overall reflectance is the element r_{12} in (7.1-4).

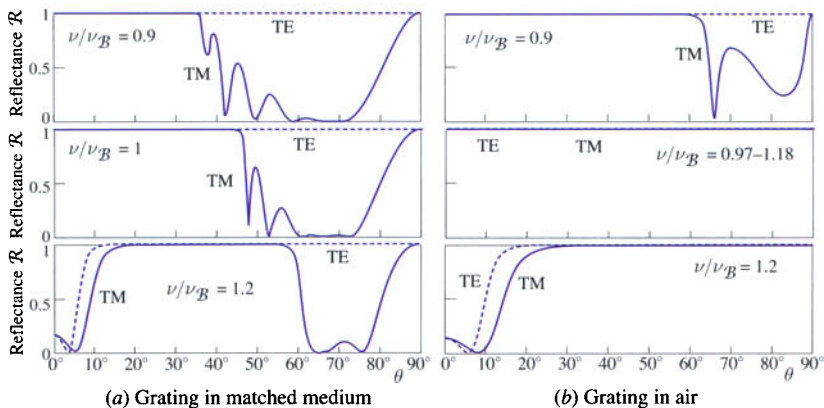(a) Grating in matched medium   (b) Grating in air

Figure 7.1-13   Intensity reflectance as a function of the angle of incidence θ at fixed frequencies for the grating described in Fig. 7.1-11. (a) Grating is placed in a matched medium ($n = n_1$). (b) Grating is placed in air ($n = 1$). In air, the grating has unity reflectance at all angles, for both TE and TM polarizations, at frequencies in the band $0.97\nu_{\mathcal{B}}$ to $1.18\nu_{\mathcal{B}}$.

7.2 ONE-DIMENSIONAL PHOTONIC CRYSTALS

One-dimensional (1D) photonic crystals are dielectric structures whose optical properties vary periodically in one direction, called the axis of periodicity, and are constant in the orthogonal directions. These structures exhibit unique optical properties, particularly when the period is of the same order of magnitude as the wavelength. If the axis of periodicity is taken to be the z direction, then optical parameters such as the permittivity $\epsilon(z)$ and the impermeability $\eta(z) = \epsilon_o/\epsilon(z)$ are periodic functions of z, satisfying

$$\eta(z + \Lambda) = \eta(z), \tag{7.2-1}$$

for all z, where Λ is the period. Wave propagation in such periodic media may be studied by solving the generalized Helmholtz equations (7.0-2), for periodic $\eta(z)$.

For an on-axis wave traveling along the z axis and polarized in the x direction, the electric and the magnetic field components E_x and H_y are functions of z, independent of x and y, so that (7.0-2) becomes

$$-\frac{d}{dz}\left[\eta(z)\frac{d}{dz}\right]H_y = \frac{\omega^2}{c_o^2}\,H_y. \tag{7.2-2}$$

For an off-axis wave, i.e., a wave traveling in an arbitrary direction in the x–z plane, the generalized Helmholtz equation has a more complex form. For example, for a TM-polarized off-axis wave, the magnetic field points in the y direction and (7.0-2) gives:

$$\left\{-\frac{\partial}{\partial z}\left[\eta(z)\frac{\partial}{\partial z}\right] + \eta(z)\frac{\partial^2}{\partial x^2}\right\}H_y = \frac{\omega^2}{c_o^2}\,H_y. \tag{7.2-3}$$

Note that (7.2-2) and (7.2-3) are cast in the form of an eigenvalue problem from which the modes $H_y(x, z)$ can be determined.

Before embarking on finding solutions to these eigenvalue problems, we first examine the conditions imposed on the propagating modes by the translational symmetry associated with the periodicity.

A. Bloch Modes

Consider first a *homogeneous medium*, which is invariant to an arbitrary translation of the coordinate system. For this medium, an optical mode is a wave that is unaltered by such a translation; it changes only by a multiplicative constant of unity magnitude (a phase factor). The plane wave $\exp(-jkz)$ is such a mode since, upon translation by a distance d, it becomes $\exp[-jk(z+d)] = \exp(-jkd)\exp(-jkz)$. The phase factor $\exp(-jkd)$ is the eigenvalue of the translation operation, as discussed in Appendix C.

On-Axis Bloch Modes

Consider now a *1D periodic medium*, which is invariant to translation by the distance Λ along the axis of periodicity. Its optical modes are waves that maintain their form upon such translation, changing only by a phase factor. These modes must have the form
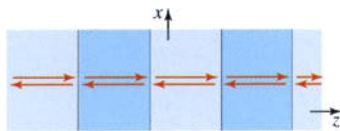
$$\boxed{U(z) = p_\kappa(z)\exp(-jKz),} \tag{7.2-4}$$

Bloch Mode

where U represents any of the field components E_x, E_y, H_x, or H_y; K is a constant, and $p_K(z)$ is a periodic function of period Λ. This form satisfies the condition that a translation Λ alters the wave by only a phase factor $\exp(-jK\Lambda)$ since the periodic function is unaltered by such translation. This optical wave is known as a **Bloch mode**, and the parameter K, which specifies the mode and its associated periodic function $p_K(z)$, is called the **Bloch wavenumber**.

The Bloch mode is thus a plane wave $\exp(-jKz)$ with propagation constant K, modulated by a periodic function $p_K(z)$, which has the character of a standing wave, as illustrated by its real part displayed in Fig. 7.2-1(a). Since a periodic function of period Λ can be expanded in a Fourier series as a superposition of harmonic functions of the form $\exp(-jmgz)$, $m = 0, \pm1, \pm2, \ldots$, with

$$g = 2\pi/\Lambda, \qquad (7.2-5)$$

it follows that the Bloch wave is a superposition of plane waves of multiple spatial frequencies $K + mg$. The fundamental spatial frequency g of the periodic structure and its harmonics mg, added to the Bloch wavenumber K, constitute the spatial spectrum of the Bloch wave, as shown in Fig. 7.2-1(b). The spatial frequency shift introduced by the periodic medium is analogous to the temporal frequency (Doppler) shift introduced by reflection from a moving object.
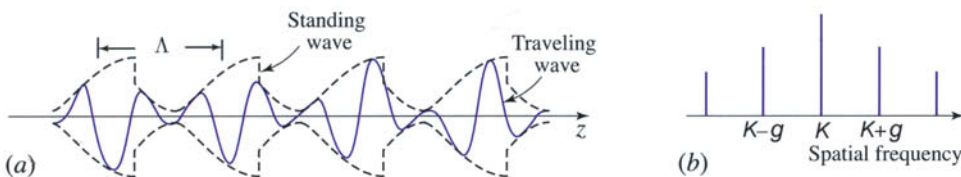

Figure 7.2-1   (a) The Bloch mode. (b) Its spatial spectrum.

Two modes with Bloch wavenumbers K and $K' = K + g$ are equivalent since they correspond to the same phase factor, $\exp(-jK'\Lambda) = \exp(-jK\Lambda)\exp(-j2\pi) = \exp(-jK\Lambda)$. This is also evident since the factor $\exp(-jgz)$ is itself periodic and can be lumped with the periodic function $p_K(z)$. Therefore, for a complete specification of all modes, we need only consider values of K in a spatial-frequency interval of width $g = 2\pi/\Lambda$. The interval $[-g/2, g/2] = [-\pi/\Lambda, \pi/\Lambda]$, known as the first **Brillouin zone**, is a commonly used construct.

Off-Axis Bloch Modes

Off-axis optical modes traveling at some angles in the x–z plane assume the Bloch form
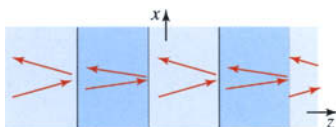
$$U(x, y, z) = p_K(z)\exp(-jKz)\exp(-jk_x x). \quad (7.2-6)$$

Off-Axis
Bloch Mode

The uniformity of the medium in the x direction constrains the x dependence of the optical mode to the harmonic form $\exp(-jk_x x)$, posing no other restriction on the transverse component k_x of the wavevector. At a location where the refractive index

is n, $k_x = nk_o \sin \theta$, where θ is the inclination angle of the wave with respect to the z axis. As the wave travels through the various layers of the inhomogeneous medium, this angle changes, but in view of Snell's law, $n \sin \theta$ and k_x are unaltered.

Normal-to-Axis Bloch Modes

When the angle of incidence in the densest medium is greater than the critical angle, the modes do not travel along the axis of periodicity (the z direction). Rather, they are normal-to-axis modes traveling along the lateral x direction that take the Bloch form (7.2-6) with $K = 0$,
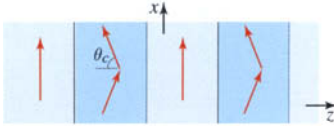
$$U(x, y, z) = p_0(z) \exp(-jk_x x), \qquad (7.2\text{-}7)$$

Normal-to-Axis
Bloch Mode

where $p_0(z)$ is a periodic function representing a standing wave along the axis of periodicity.

Eigenvalue Problem, Dispersion Relation, and Photonic Bandgaps

Now that we have established the mathematical form of the modes, as imposed by the translational symmetry of the periodic medium, the next step is to solve the eigenvalue problem described by the generalized Helmholtz equation. For a mode with a Bloch wavenumber K, the eigenvalues ω^2/c_o^2 provide a discrete set of frequencies ω. These values are used to construct the ω-K dispersion relation. The eigenfunctions help us determine the Bloch periodic functions $p_K(z)$ for each of the values of ω associated with each K.

The ω-K relation is a periodic multivalued function of K with period g, the fundamental spatial frequency of the periodic structure; it is often plotted over the Brillouin zone $[-g/2 < k \leq g/2]$, as illustrated schematically in Fig. 7.2-2(a). When visualized as a monotonically increasing function of k, it appears as a continuous function with discrete jumps at values of K equal to integer multiples of $g/2$. These discontinuities correspond to the photonic bandgaps, which are spectral bands not crossed by the dispersion lines, so that no propagating modes exist.

The origin of the discontinuities in the dispersion relation lies in the special symmetry that emerges when $k = g/2$, i.e., when the period of the traveling wave equals exactly half a period of the periodic medium. Consider the two modes with $k = \pm g/2$ and Bloch periodic functions $p_K(z) = p_{\pm g/2}(z)$. Since these modes travel with the same wavenumber, but in opposite directions, i.e. see inverted versions of the medium, $p_{-g/2}(z) = p_{g/2}(-z)$. But these two modes are in fact one and the same, because their Bloch wavenumbers differ by g. It therefore follows that at the edge of a Brillouin zone, there are two Bloch periodic functions that are inverted versions of one another. Since the medium is inhomogeneous or piecewise homogeneous within a unit cell, these two distinct functions interact with the medium differently, and therefore have two distinct eigenvalues, i.e., distinct values of ω. This explains the discontinuity that emerges as the continuous ω-K line crosses the boundary of the Brillouin zone. A similar argument explains the discontinuities that occur when K equals other integer multiples of $g/2$.

The variational principle (see Appendix C) is helpful in pointing out certain features of these eigenfunctions. Based on this principle, the eigenfunctions of a Hermitian operator are orthogonal distributions that minimize the variational energy. The variational energy associated with the linear operator $\mathcal{L}$ in the eigenvalue equation (7.0-2) is $E_v = \frac{1}{2}(\mathbf{H}, \mathcal{L}\mathbf{H})/(\mathbf{H}, \mathbf{H})$. By use of Maxwell's equations, it can be shown that $(\mathbf{H}, \mathcal{L}\mathbf{H}) = (\mathbf{H}, \nabla \times [\eta(\mathbf{r}) \nabla \times \mathbf{H}]) = \int |\mathbf{D}(\mathbf{r})|^2/\epsilon(\mathbf{r})d\mathbf{r}$, so that minimization of E_v is achieved

by distributions for which higher displacement fields $\mathbf{D}(\mathbf{r})$ are located at positions of lower $1/\epsilon(\mathbf{r})$, i.e. higher refractive index. For example, if the periodic medium is made of two alternating dielectric layers, as illustrated in Fig. 7.2-2(b), then at a discontinuity the eigenfunction of the lower frequency concentrates its displacement field in the layer with the greater refractive index, whereas the eigenfunction of the higher frequency has an inverted distribution for which the displacement field is concentrated in the layer with the lower refractive index.
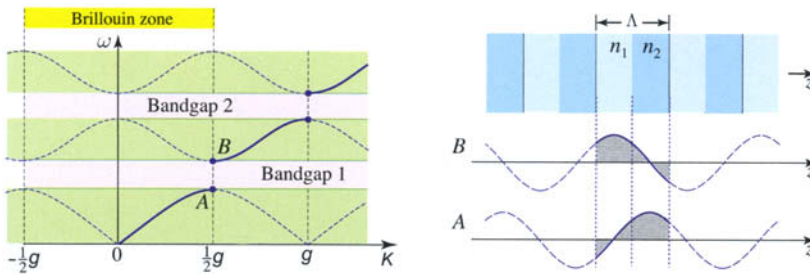

Figure 7.2-2   (a) The dispersion relation is a multivalued periodic function with period $g = 2\pi/\Lambda$ and discontinuities at k equals integer multiples of $g/2$. (b) Bloch functions at the points A and B at the edge of the Brillouin zone for an alternating dielectric-layer periodic medium with $n_2 > n_1$.

The challenging problem now is the solution of the eigenvalue problem associated with the Helmholtz equation. There are two approaches:

■ The first approach is based on expanding the periodic function $\eta(z)$ of the medium and the periodic function $p_K(z)$ of the Bloch mode in Fourier series and converting the Helmholtz differential equation into a set of algebraic equation cast in the form of a matrix eigenvalue problem, which are solved numerically. This approach is called the **Fourier Optics** approach.

■ The second approach is applicable to layered (piecewise homogeneous) media with planar boundaries. Instead of solving the Helmholtz equation, we make direct use of the laws of propagation and reflection/refraction at boundaries, which are known consequences of Maxwell's equations. We then use the matrix methods developed for multilayer media in Sec. 7.1A and applied to Bragg gratings in Sec. 7.1C. This **Matrix Optics** approach leads to a 2×2 matrix eigenvalue problem from which the dispersion relation and the Bloch modes are determined.

The matrix-optics approach is discussed next, and the Fourier-optics approach is examined in Sec. 7.2C.

B. Matrix Optics of Periodic Media

A one-dimensional periodic medium comprises identical segments, called **unit cells**, that are repeated periodically along one direction (the z axis) and separated by the period Λ (Fig. 7.2-3). Each unit cell contains a succession of lossless dielectric layers or partially reflective mirrors in some order, forming a reciprocal system represented by a generic unimodular wave- transfer matrix

$$\mathbf{M}_o = \begin{bmatrix} 1/t^* & r/t \\ r^*/t^* & 1/t \end{bmatrix}, \tag{7.2-8}$$

where t and r are complex amplitude transmittance and reflectance satisfying the conditions set forth in (7.1-15), and $\mathcal{T} = |t|^2$ and $\mathcal{R} = |r|^2$ are the corresponding intensity

transmittance and reflectance. The medium is a Bragg grating, like that described in Sec. 7.1C, with an infinite number of segments. A wave traveling through the medium undergoes multiple transmissions and reflections that add up to one forward and one backward wave at every plane. We now use the matrix method developed in Sec. 7.1A to determine the Bloch modes.
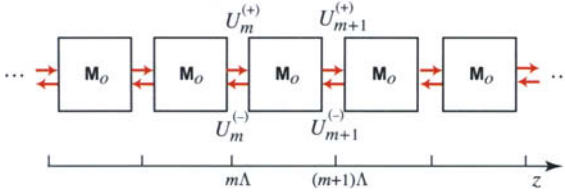

Figure 7.2-3 Wave-transfer matrix representation of a periodic medium.

Let $\{U_m^{(\pm)}\}$ be the complex amplitudes of the forward and backward waves at the initial position $z = m\Lambda$ of unit cell m. Knowing these amplitudes, the amplitudes elsewhere within the cell can be determined by straightforward application of the appropriate wave-transfer matrices, as described in Sec. 7.1. We therefore direct our attention to the dynamics of the amplitudes $\{U_m^{(\pm)}\}$ as they vary from one cell to the next. These dynamics are described by the recurrence relations

$$\begin{bmatrix} U_{m+1}^{(+)} \\ U_{m+1}^{(-)} \end{bmatrix} = \mathbf{M}_o \begin{bmatrix} U_m^{(+)} \\ U_m^{(-)} \end{bmatrix}, \qquad (7.2\text{-}9)$$

which can be used to determine the amplitudes at a particular cell if the amplitudes at the previous cell are known.

Eigenvalue Problem and Bloch Modes

By definition, the modes of the periodic medium are self-reproducing waves, for which

$$\begin{bmatrix} U_{m+1}^{(+)} \\ U_{m+1}^{(-)} \end{bmatrix} = e^{-j\Phi} \begin{bmatrix} U_m^{(+)} \\ U_m^{(-)} \end{bmatrix}, \qquad m = 1, 2, \ldots; \qquad (7.2\text{-}10)$$

after transmission through a distance Λ (in this case a unit cell), the magnitudes of the forward and backward waves remain unchanged and the phases are altered by a common shift Φ, called the **Bloch phase**. The corresponding Bloch wavenumber is $K = \Phi/\Lambda$, so that

$$\boxed{\Phi = K\Lambda.} \qquad (7.2\text{-}11)$$
Bloch Phase

Determination of the complex amplitudes $U_m^{(\pm)}$ and the phase $\Phi = K\Lambda$ that satisfy the self-reproduction condition (7.2-10) can be cast as an eigenvalue problem. This is accomplished by using (7.2-9) with $m = 0$ to write (7.2-10) in the form

$$\mathbf{M}_o \begin{bmatrix} U_0^{(+)} \\ U_0^{(-)} \end{bmatrix} = e^{-j\Phi} \begin{bmatrix} U_0^{(+)} \\ U_0^{(-)} \end{bmatrix}. \qquad (7.2\text{-}12)$$

This is an eigenvalue problem for the 2×2 unit-cell matrix $\mathbf{M}_o$. The factor $e^{-j\Phi}$ is the eigenvalue and the vector with components $U_0^{(+)}$ and $U_0^{(-)}$ is the eigenvector.

The eigenvalues are determined by equating the determinant of the matrix $\mathbf{M}_o - e^{-j\Phi}\mathbf{I}$ to zero. Noting that $|t|^2 + |r|^2 = 1$, the solution to the ensuing quadratic equation yields $e^{-j\Phi} = \frac{1}{2}(1/t + 1/t^*) \pm j\{1 - [\frac{1}{2}(1/t + 1/t^*)]^2\}^{1/2}$, from which

$$\boxed{\cos\Phi = \mathrm{Re}\left\{\frac{1}{t}\right\}.}$$

(7.2-13)

Equation (7.2-13) is identical to (7.1-49) for the Bragg grating. This is gratifying inasmuch as the periodic medium at hand is an extended Bragg grating with an infinite number of segments.

Since $\mathbf{M}_o$ is a 2×2 matrix, it has two eigenvalues. Hence, only two of the multiple solutions of (7.2-13) are independent. Since the $\cos^{-1}(\cdot)$ function is even, the two solutions within the interval $[-\pi, \pi]$ have equal magnitudes and opposite signs. They correspond to Bloch modes traveling in the forward and backward directions. Other solutions obtained by adding multiples of 2π are not independent since they are irrelevant to the phase factor $e^{-j\Phi}$.

The associated eigenvectors of $\mathbf{M}_o$ are therefore

$$\begin{bmatrix} U_0^{(+)} \\ U_0^{(-)} \end{bmatrix} \propto \begin{bmatrix} r/t \\ e^{-j\Phi} - 1/t^* \end{bmatrix},$$

(7.2-14)

as can be ascertained by operating on the right-hand side of (7.2-14) with the $\mathbf{M}_o$ matrix; the result is again the right-hand side of (7.2-14) to within a constant.

The periodic function $p_K(z)$ associated with the Bloch wave can be determined by propagating the amplitudes $U_0^{(+)}$ and $U_0^{(-)}$ through the unit cell. For example, if the initial layer in the unit cell is a homogeneous medium of refractive index n_1 and width d_1, then the wave at distance z into this layer is

$$p_K(z)\, e^{-jKz} = U_0^{(+)} e^{-jn_1 k_0 z} + U_0^{(-)} e^{jn_1 k_0 z}, \quad 0 < z < d_1.$$

(7.2-15)

Using (7.2-14) and (7.2-11), (7.2-15) then provides

$$p_K(z) \propto \left[-r e^{-jn_1 k_0 z} + (e^{-jK\Lambda} - 1)\, e^{jn_1 k_0 z} \right] e^{jKz}, \quad 0 < z < d_1.$$

(7.2-16)

The waves in (7.2-16) may be propagated further into the subsequent layers within the cell by using the appropriate $\mathbf{M}$ matrices.

Dispersion Relation and Photonic Band Structure

The **dispersion relation** is an equation relating the Bloch wavenumber K and the angular frequency ω. Equation (7.2-13), which provides the eigenvalues $\exp(-j\Phi)$ of the unit-cell matrix, is the progenitor of the dispersion relation for the 1D periodic medium. The phase $\Phi = K\Lambda$ is proportional to K, and $t = t(\omega)$ is related to ω through the phase delay associated with propagation through the unit cell, so that (7.2-13), written in the form

$$\boxed{\cos\left(2\pi \frac{K}{g}\right) = \mathrm{Re}\left\{\frac{1}{t(\omega)}\right\},}$$

(7.2-17)
Dispersion Relation

is the $\omega - K$ dispersion relation. Here, $g = 2\pi/\Lambda$ is the fundamental spatial frequency of the periodic medium.

The function $\cos(2\pi K/g)$ is a periodic function of K of period $g = 2\pi/\Lambda$, so that for a given ω, (7.2-17) has multiple solutions. However, solutions separated by the period g are not independent since they lead to identical Bloch waves. It is therefore common to limit the domain of the dispersion relation to a period with values of K in the interval $[-g/2, g/2]$ or $[-\pi/\Lambda, \pi/\Lambda]$, which is the Brillouin zone. This corresponds precisely to limiting the phase Φ to the interval $[-\pi, \pi]$. Also, since $\cos(2\pi K/g)$ is an even function of K, at each value ω there are two independent values of K of equal magnitudes and opposite signs within the Brillouin zone. They correspond to independent Bloch modes traveling in the forward and backward directions.

The dispersion relation exhibits multiple spectral bands classified into two regimes:

- **Propagation regime**. Spectral bands within which K is real correspond to propagating modes. Defined by the condition $|\operatorname{Re}\{1/t(\omega)\}| \leq 1$, these bands are numbered, 1, 2, ..., starting with the lowest-frequency band.
- **Photonic bandgap regime**. Spectral bands within which K is complex correspond to evanescent waves that are rapidly attenuated. Defined by the condition $|\operatorname{Re}\{1/t(\omega)\}| > 1$, these bands correspond to the stop bands of the diffraction grating discussed in Sec. 7.1C. They are also called **photonic bandgaps (PBG)** or **forbidden gaps** since propagating modes do not exist.

The dispersion relation is often plotted with K measured in units of $g = 2\pi/\Lambda$, the fundamental spatial frequency of the periodic structure, whereas ω is measured in units of the Bragg frequency $\omega_B = \pi c/\Lambda$, where $c = c_o/\bar{n}$ and $\bar{n}$ is the average refractive index of the periodic medium. The ratio $\omega_B/(g/2) = c$, which is the slope of the dispersion relation $\omega = cK$ for propagation in a homogeneous medium with the average refractive index.

EXAMPLE 7.2-1. *Periodic Stack of Partially Reflective Mirrors.* The dispersion relation for a wave traveling along the axis of a periodic stack of identical partially reflective lossless mirrors with intensity reflectance $|r|^2$ and intensity transmittance $|t|^2 = 1 - |r|^2$, separated by a distance Λ, is determined directly from Example 7.1-8. Using the results obtained there, namely $t = |t|e^{j\varphi}$ with $\varphi = nk_o\Lambda = (\omega/c)\Lambda$, in conjunction with (7.2-13), provides the dispersion relation

$$\cos\left(2\pi\frac{K}{g}\right) = \frac{1}{|t|}\cos\left(\pi\frac{\omega}{\omega_B}\right), \qquad (7.2\text{-}18)$$

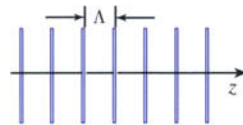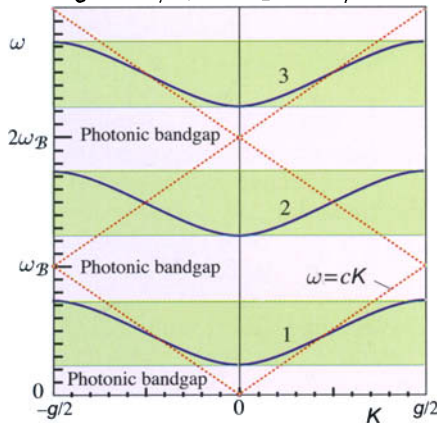where $g = 2\pi/\Lambda$, and $\omega_B = c\pi/\Lambda$ is the Bragg frequency. This result is plotted in Fig. 7.2-4.

Figure 7.2-4 Dispersion diagram of a periodic set of mirrors, each with intensity transmittance $|t|^2 = 0.5$, separated by a distance Λ. Here, $\omega_B = \pi c/\Lambda$ and $g = 2\pi/\Lambda$. The dotted straight lines represent propagation in a homogeneous medium for which $\omega/K = \omega_B/(g/2) = c$.

The photonic bandgaps, which correspond to frequency regions where (7.2-18) does not admit a real solution, are centered at $\omega_\mathcal{B}$, $2\omega_\mathcal{B}$, ... These frequency regions do not permit propagating modes; rather, they correspond to the stop bands that exhibit unity reflectance in Fig. 7.1-10. In this system, the onset of the lowest photonic bandgap is at $\omega = 0$.

EXAMPLE 7.2-2.   *Alternating Dielectric Layers.* A periodic medium comprises alternating dielectric layers of refractive indexes n_1 and n_2, with corresponding widths d_1 and d_2, and period $\Lambda = d_1 + d_2$. This system is the dielectric Bragg grating described in Example 7.1-9 with $N = \infty$. For a wave traveling along the axis of periodicity, $\mathrm{Re}\{1/t\} = \mathrm{Re}\{A\}$ is given by (7.1-61). Using the relations $\varphi_1 + \varphi_2 = k_o(n_1 d_1 + n_2 d_2) = \pi\omega/\omega_\mathcal{B}$ and $\varphi_1 - \varphi_2 = \zeta\pi\omega/\omega_\mathcal{B}$, where $\omega_\mathcal{B} = (c_o/\bar{n})(\pi/\Lambda)$ is the Bragg frequency, $\bar{n} = (n_1 d_1 + n_2 d_2)/\Lambda$ is the average refractive index and $\zeta = (n_1 d_1 - n_2 d_2)/(n_1 d_1 + n_2 d_2)$, (7.2-13) provides the dispersion relation

$$\cos\left(2\pi\frac{K}{g}\right) = \frac{1}{\mathsf{t}_{12}\mathsf{t}_{21}}\left[\cos\left(\pi\frac{\omega}{\omega_\mathcal{B}}\right) - |\mathsf{r}_{12}|^2\cos\left(\pi\zeta\frac{\omega}{\omega_\mathcal{B}}\right)\right], \qquad (7.2\text{-}19)$$

where $\mathsf{t}_{12}\mathsf{t}_{21} = 4n_1 n_2/(n_1 + n_2)^2$ and $|\mathsf{r}_{12}|^2 = (n_2 - n_1)^2/(n_1 + n_2)^2$.

An example of this dispersion relation is plotted in Fig. 7.2-5 for dielectric materials with $n_1 = 1.5$ and $n_2 = 3.5$, and $d_1 = d_2$. As with the periodic stack of partially reflective mirrors considered in Example 7.2-1, the photonic bandgaps are centered at the frequencies $\omega_\mathcal{B}$ and its multiples, and occur at either the center of the Brillouin zone ($K = 0$) or at its edge ($K = g/2$). In this case, however, the frequency region surrounding $\omega = 0$ admits propagating modes instead of a forbidden gap. Dielectric materials with lower contrast have bandgaps of smaller width, but the bandgaps exist no matter how small the contrast.
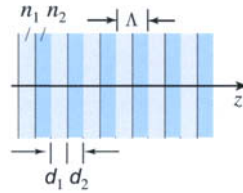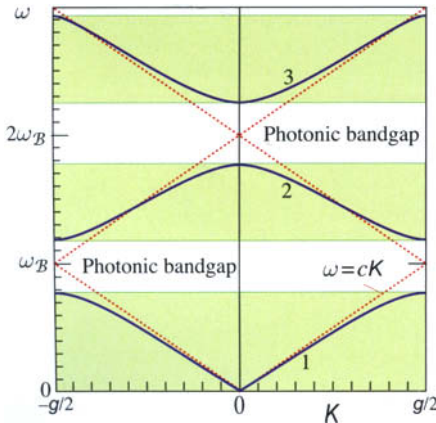

Figure 7.2-5 Dispersion diagram of an alternating-layer periodic dielectric medium with $n_1 = 1.5$ and $n_2 = 3.5$, and $d_1 = d_2$. Here, $\omega_\mathcal{B} = \pi c_o/\Lambda\bar{n}$ and $g = 2\pi/\Lambda$. The dotted straight lines represent propagation in a homogeneous medium of mean refractive index $\bar{n}$, so that $\omega/K = \omega_\mathcal{B}/(g/2) = c_o/\bar{n} = c$.

Phase and Group Velocities

The propagation constant K corresponds to a phase velocity ω/K and an effective refractive index $n_{\mathrm{eff}} = c_o K/\omega$. The group velocity $v = d\omega/dK$, which governs pulse propagation in the medium, is associated with an effective group index $N_{\mathrm{eff}} = c_o dK/d\omega$ (see Sec.5.6). These indexes can be determined at any point on the ω-K dispersion curve by finding the slope $d\omega/dK$, and the ratio ω/K, i.e., the slope of a line joining the point with the origin. Figure 7.2-6 is a schematic illustration of a dispersion relation of an alternating-layer dielectric periodic medium, together with the effective index and group index, at frequencies extending over two photonic bands with a photonic bandgap in-between.

At low frequencies within the first photonic band, n_{eff} is approximately equal to the average refractive index $\bar{n}$. This is expected since at long wavelengths the material
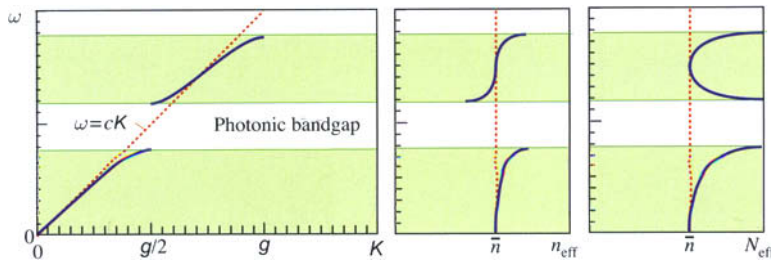
Figure 7.2-6   Frequency dependence of the effective refractive index n_{eff}, which determines the phase velocity, and the effective group index N_{eff}, which determines the group velocity.

behaves as a homogeneous medium with the average refractive index. With increase of frequency, n_{eff} increases above $\bar{n}$, reaching its highest value at the band edge. At the bottom of the second band, n_{eff} is smaller than $\bar{n}$ but increases at higher frequencies, approaching $\bar{n}$ in the middle of the band.

This drop of n_{eff} from a value above average just below the bandgap to a value below average just above the bandgap is attributed to the significantly different spatial distributions of the corresponding Bloch modes, which are orthogonal. The mode at the top of the lower band, has greater energy in the dielectric layers with the higher refractive index, so that its effective index is greater than the average. For the mode at the bottom of the upper band, greater energy is localized in the layers with the lower refractive index, and the effective index is therefore lower than the average.

The frequency dependence of the effective group index follows a different pattern, as shown in Fig. 7.2-6. As the edges of the bandgap are approached, from below or above, this index increases substantially, so that the group velocity is much smaller, i.e., optical pulses are very slow near the edges of the bandgap.

Off-Axis Dispersion Relation and Band Structure

The dispersion relation for off-axis waves may be determined by using the same equation, $\cos(K\Lambda) = \text{Re}\{1/\text{t}(\omega)\}$, where $\text{Re}\{1/\text{t}(\omega)\}$ now depends on the angles of incidence within the layers of each segment and on the state of polarization (TE or TM). For example, for a periodic medium made of alternating dielectric layers, $\text{Re}\{1/\text{t}(\omega)\}$ takes the more general form in (7.1-62).

Since the same transverse component k_x of the wavevector determines the angles of incidence at the two layers ($k_x = n_1 k_o \sin\theta_1 = n_2 k_o \sin\theta_2$), it is more convenient to express the dispersion relation as a function of k_x, in the form of a three-dimensional surface $\omega = \omega(K, k_x)$. Every value of k_x yields a dispersion diagram with bands and bandgaps similar to those of Fig. 7.2-5.

A simpler representation of the $\omega(K, k_x)$ 3D surface is the **projected dispersion diagram**, which displays in a two-dimensional plot of the edges of the bands and bandgaps at each value of k_x, for both TE and TM polarizations, as illustrated in Fig. 7.2-7. This figure is constructed by determining the ranges of angular frequencies over which photonic bands and bandgaps exist in the dispersion diagram for a particular value of k_x, and then projecting these onto corresponding vertical lines at that value of k_x in the projected dispersion diagram. The loci of all such vertical lines for the bands at different values of k_x correspond to the shaded (green) areas displayed in Fig. 7.2-7; the unshaded (white) areas represent the bandgaps.

In this diagram, each angle of incidence is represented by a straight line passing through the origin. For example, the incidence angle θ_1 in layer 1 corresponds to the line $k_x = (\omega/c_1)\sin\theta_1$, i.e., $\omega = (c_1/\sin\theta_1)k_x$, where $c_1 = c_o/n_1$. The line $\omega = c_1 k_x$, called the **light line** corresponds to $\theta_1 = 90°$. Similar lines may be drawn for
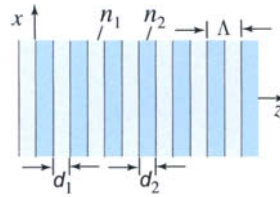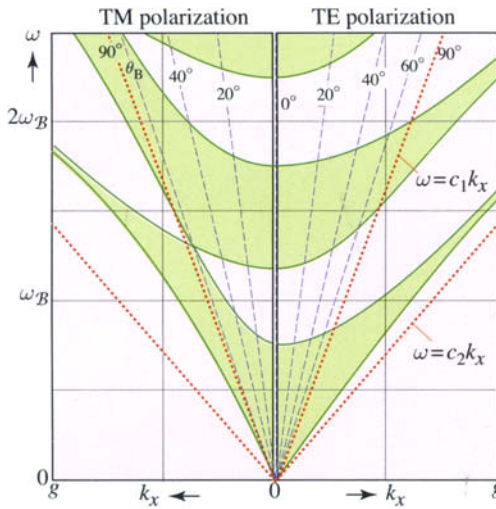
Figure 7.2-7   Projected dispersion diagram for an alternating-layer periodic dielectric medium with $n_1 = 1.5$, $n_2 = 3.5$, and $d_1 = d_2 = \Lambda/2$. Here, $\omega_\mathcal{B} = \pi c_o/\Lambda \bar{n}$ and $g = 2\pi/\Lambda$. Photonic bands are shaded (green). The dashed lines represent fixed angles of incidence θ_1 in layer 1, including the Brewster angle $\theta_B = 66.8°$. Points within the region bounded by the light lines $\omega = c_1 k_x$ and $\omega = c_2 k_x$ represent normal-to-axis waves.

the incidence angles in medium 2; Fig. 7.2-7 shows only the light line $\omega = c_2 k_x$, assuming that $n_2 > n_1$, i.e., $c_2 < c_1$. Points in the region bounded by the two light lines represent normal-to- axis modes, which travel in the lateral direction by undergoing total reflection in the denser medium (medium 2).

The question arises as to whether there exists a frequency range over which propagation is forbidden at all angles of incidence θ_1 and θ_2 and for both polarizations? This could occur if the forbidden gaps at all values of k_x between the lines $k_x = 0$ and $k_x = \omega/c_2$, and for both polarizations, were to align in such a way as to create a common or **photonic bandgap**. This is clearly not the case in the example in Fig. 7.2-7. It turns out that this is not possible; complete photonic bandgaps cannot exist within 1D periodic structures. However, they can occur in 2D and 3D periodic structures, as we shall see in Sec. 7.3.

Indeed, there is one special case in which a photonic bandgap cannot occur at all, and that is an oblique TM wave propagating at the Brewster angle $\theta_B = \tan^{-1}(n_2/n_1)$ in layer 1. As shown in Fig. 7.2-7, the line at the Brewster angle does not pass through a gap. This is not surprising since at this angle, the reflectance of a unit cell is zero, and the forward and backward waves are uncoupled so that the collective effect that leads to total reflection is absent.

C. Fourier Optics of Periodic Media

The matrix analysis of periodic media presented in the previous section is applicable to layered (i.e., piecewise homogeneous) media. A more general approach, applicable for arbitrary periodic media, including continuous media, is based on a Fourier-series representation of periodic functions and conversion of the Helmholtz equation into a set of algebraic equations whose solution provides the dispersion relation and the Bloch modes. This approach can also be generalized to 2D and 3D periodic media, as will be shown in Sec. 7.3.

A wave traveling along the axis of a 1D periodic medium (the z axis) and polarized in the x direction is described by the generalized Helmholtz equation (7.2-2). Since $\eta(z)$ is periodic with period Λ, it can be expanded in a Fourier series,

$$\eta(z) = \sum_{\ell=-\infty}^{\infty} \eta_\ell \exp(-j\ell g\, z), \qquad (7.2\text{-}20)$$

where $g = 2\pi/\Lambda$ is the spatial frequency (rad/mm) of the periodic structure and η_ℓ is the Fourier coefficient representing the ℓth harmonic. The impermeability $\eta(z)$ is real, so that $\eta_{-\ell} = \eta_\ell^*$.

The periodic portion of the Bloch wave $p_K(z)$ in (7.2-4) may also be expanded in a Fourier series,

$$p_K(z) = \sum_{m=-\infty}^{\infty} C_m \exp\left(-jm g\,z\right), \qquad (7.2\text{-}21)$$

whereupon the Bloch wave representation of the magnetic field may be written as

$$H_y(z) = \sum_{m=-\infty}^{\infty} C_m \exp\left[-j(K + m g)z\right]. \qquad (7.2\text{-}22)$$

For brevity, the dependence of the Fourier coefficients $\{C_m\}$ on the Bloch wavenumber K is suppressed. Substituting these expansions into the Helmholtz equation (7.2-2) and equating harmonic terms of the same spatial frequency, we obtain

$$\sum_{\ell=-\infty}^{\infty} F_{m\ell} C_\ell = \frac{\omega^2}{c_o^2} C_m, \quad F_{m\ell} = (K + m g)(K + \ell g)\,\eta_{m-\ell}, \qquad (7.2\text{-}23)$$

where $m = 0, \pm 1, \pm 2, \ldots$.

The differential equation (7.2-2) has now been converted into a set of linear equations (7.2-23) for the unknown Fourier coefficients $\{C_m\}$. These equations may be cast in the form of a matrix eigenvalue problem. For each K, the eigenvalues ω^2/c_o^2 correspond to multiple values of ω, from which the ω-K dispersion relation may be constructed. The eigenvectors are sets of $\{C_m\}$ coefficients, which determine the periodic function $p_K(z)$ of the Bloch mode for each K.

Posed as an eigenvalue problem for a matrix $\mathbf{F}$ with elements $F_{m\ell}$, this set of coupled equations may be solved using standard numerical techniques. Since $\eta_{m-\ell} = \eta_{\ell-m}^*$, the matrix $\mathbf{F}$ is Hermitian, i.e., $F_{m\ell} = F_{\ell m}^*$. Note that if we were to use the electric-field Helmholtz equation instead of the magnetic-field Helmholtz equation (7.2-2), we would obtain another matrix representation of the eigenvalue problem, but the matrix would be non-Hermitian, and therefore more difficult to solve. This is why we elected to work with the Helmholtz equation for the magnetic field.[†]

Approximate Solution of the Eigenvalue Problem

In (7.2-23), the harmonics of the optical wave are coupled via the harmonics of the periodic medium. An optical-wave harmonic of spatial frequency $K + \ell g$ mixes with a medium harmonic of spatial frequency $(m - \ell)g$ and contributes to the optical-wave harmonic of spatial frequency $(K + \ell g) + (m - \ell)g = K + m g$.

The conditions under which strong coupling emerges can be determined by separating out the mth term in (7.2-23), which leads to

$$C_m = \sum_{\ell \neq m} \frac{\eta_{m-\ell}}{\eta_o} \frac{(K + \ell g)(K + m g)}{(\bar{n}\omega/c_o)^2 - (K + m g)^2} C_\ell, \quad m = 0, \pm 1, \pm 2, \ldots, \qquad (7.2\text{-}24)$$

[†] It can be shown that the differential operator in the generalized Helmholtz equation, (7.0-2), is a Hermitian operator, but that for the electric field is non-Hermitian.

where $\bar{n} = 1/\sqrt{\eta_0}$ is an average refractive index of the medium. Strong coupling between the mth harmonic of the wave and other harmonics exists if the denominator in (7.2-24) is small, i.e.,

$$\omega \bar{n}/c_o \approx |K + mg|. \tag{7.2-25}$$

This equation represents a resonance condition for interaction between the harmonics. It can also be regarded as a **phase matching condition**.

Figure 7.2-8 is a plot of (7.2-25) as an equality. For each value of m, the ω-K relation is a V-shaped curve. The intersection points of these curves represent common values of ω and K at which (7.2-25) is simultaneously satisfied for two harmonics. The intersections between the $m = 0$ curve (dashed) and the curves for $m = -1, m = -2$, ..., are marked by filled circles; they correspond to the lowest-order bandgaps 1, 2, ..., respectively. At each intersection point, K is an integer multiple of $\frac{1}{2}g$, and ω is an integer multiple of the Bragg frequency $\omega_B = (c_o/\bar{n})g/2$ or $\omega_B/2\pi = \nu_B = (c_o/\bar{n})/2\Lambda$. This corresponds to the Bragg wavelength $\lambda_B = 2\Lambda$ in the medium, and therefore to total reflection. Unmarked intersections in Fig. 7.2-8 are not independent since each of these has the same ω as a marked intersection, and a value of K differing by a reciprocal lattice constant g.
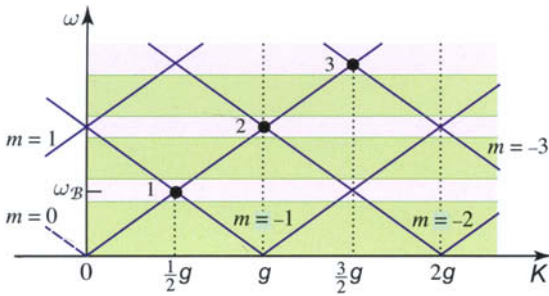

Figure 7.2-8 Plot of (7.2-25), as an equality, for various values of m. The $m = 0$ curve is indicated as dashed. Strong coupling between the harmonics of the optical wave and those of the medium occurs at the intersection points 1, 2,..., which correspond to the lowest-order bandgaps.

The lowest-order bandgap occurs at the intersection of the $m = 0$ and $m = -1$ curves (point 1 in Fig. 7.2-8). In this case, only the coefficients C_0 and C_{-1} are strongly coupled, so that (7.2-24) yields two coupled equations

$$C_0 = \frac{\eta_1}{\eta_0} \frac{(K - g)K}{\omega^2 \bar{n}^2/c_o^2 - K^2} C_{-1}, \tag{7.2-26}$$

$$C_{-1} = \frac{\eta_1^*}{\eta_0} \frac{K(K - g)}{\omega^2 \bar{n}^2/c_o^2 - (K - g)^2} C_0, \tag{7.2-27}$$

where $\eta_{-1} = \eta_1^*$. These equations are self-consistent if

$$\boxed{\frac{|\eta_1|^2}{\eta_0^2} K^2(K - g)^2 = \left[\omega^2 \frac{\bar{n}^2}{c_o^2} - K^2\right]\left[\omega^2 \frac{\bar{n}^2}{c_o^2} - (K - g)^2\right].} \tag{7.2-28}$$

Dispersion Relation

A plot of this equation (Fig. 7.2-9) yields the ω-K dispersion relation near the edge of the bandgap, where the equation is valid. For $K = \frac{1}{2}g$, (7.2-28) yields two frequencies,

$$\omega_\pm = \omega_B \sqrt{1 \pm |\eta_1|/\eta_0}, \tag{7.2-29}$$

representing the edges of the first photonic bandgap. The center of the bandgap is at the Bragg frequency $\omega_{\mathcal{B}} = (c_o/\bar{n})(g/2) = (\pi/\Lambda)(c_o/\bar{n})$. The ratio of the gap width to the midgap frequency, which is called the **gap-midgap ratio**, grows with increasing impermeability contrast ratio $|\eta_1|/\eta_0$.
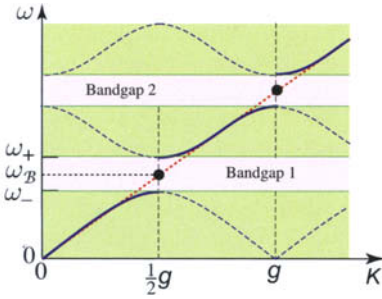

Figure 7.2-9 Dispersion relation in the vicinity of photonic bandgaps.

A similar procedure can be followed to determine the spectral width of higher-order bandgaps. The width of the mth bandgap is determined by a formula identical to (7.2-29), but the ratio $|\eta_m|/\eta_0$ replaces $|\eta_1|/\eta_0$, so that higher bandgaps are governed by higher spatial harmonics of the periodic function $\eta(z)$.

Off-Axis Waves

The dispersion relation for off-axis waves may be determined by use of the same Fourier expansion technique. For a TM-polarized off-axis wave traveling in an arbitrary direction in the x–z plane, the Helmholtz equation is given by (7.2-3). The Bloch wave is a generalization of (7.2-22) obtained via (7.2-6),

$$H_y(z) = \sum_{m=-\infty}^{\infty} C_m \exp\left[-j(K + mg)z\right] \exp(-jk_x x). \qquad (7.2\text{-}30)$$

Carrying out calculations similar to the on-axis case, leads to the following set of algebraic equations for the C_m coefficients:

$$\sum_{\ell=-\infty}^{\infty} F_{m\ell} C_\ell = \frac{\omega^2}{c_o^2} C_m, \quad F_{m\ell} = [(K + \ell g)(K + mg) + k_x^2]\eta_{m-\ell}. \qquad (7.2\text{-}31)$$

Equation (7.2-31) is a generalization of (7.2-23) for the off-axis wave. The dispersion relation may be determined by solving this matrix eigenvalue problem for the set of frequencies ω associated with each pair of values of K and k_x.

D. Boundaries Between Periodic and Homogeneous Media

The study of light wave propagation in periodic media has so far been limited to determining the dispersion relation and its associated band structure, as well as estimating the phase and group velocity of such waves. By definition, the periodic medium extend indefinitely in all directions. The next step is to examine reflection and transmission at boundaries between periodic and homogeneous media. We first examine reflection from a single boundary and subsequently consider a slab of periodic medium embedded in a homogeneous medium. Other configurations made of homogeneous structures such slabs or holes embedded in extended periodic media are described in Sec. 9.4 and Sec. 10.4D.

Omnidirectional Reflection at a Single Boundary

We examine the reflection and transmission of an optical wave at the boundary between a semi-infinite homogeneous medium and a semi-infinite one-dimensional periodic medium, as portrayed in Fig. 7.2-10. We demonstrate that, under certain conditions and within a specified range of angular frequencies, the periodic medium acts as a perfect mirror, totally reflecting waves incident from any direction and with any polarization!

Wave transmission and reflection at the boundary between two media is governed by the phase-matching condition. At the boundary between two homogeneous media, for example, the transverse components of the wavevector k_x must be the same on both sides of the boundary. Since $k_x = k \sin \theta = (\omega/c_o)n \sin \theta$, this condition means that the product $n \sin \theta$ is invariant. This is the origin of Snell's law of refraction, as explained in Sec. 2.4A.

Similarly, for a wave incident from a homogeneous medium into a one-dimensional periodic medium, k_x must remain the same. Thus, if the incident wave has angular frequency ω and angle of incidence θ, we have $k_x = (\omega/c_o)n \sin \theta$, where n is the refractive index of the homogeneous medium. Knowing k_x and ω, we can use the dispersion relation $\omega = \omega(K, k_x)$ for the periodic medium at the appropriate polarization to determine the Bloch wavenumber K. If the angular frequency ω lies within a forbidden gap at this value of k_x, the incident wave will not propagate into the periodic medium but will, instead, be totally reflected. This process is repeated for all frequencies, angles of incidence, and polarizations of the incident wave.

We now consider the possibility that the boundary acts as an omnidirectional reflector (a perfect mirror). For this purpose, we use the projected dispersion diagram, which displays the bandgaps for each value of k_x, as illustrated in the example provided in Fig. 7.2-10. On the same diagram, we delineate by a red dashed line the ω-k_x region that can be accessed by waves entering from the homogeneous medium. This region is defined by the equation $k_x = (\omega/c_o)n \sin \theta$, which dictates that $k_x < (\omega/c_o)n$ or $\omega > (c_o/n)k_x$; it is thus bounded by the line $\omega = (c_o/n)k_x$, or $\omega/\omega_{\mathcal{B}} = (\bar{n}/n)[k_x/(g/2)]$, known as the light line. This line corresponds to an angle $\theta = 90°$ in the surrounding medium.

Figure 7.2-10 reproduces Fig. 7.2-7 with the light lines added, and the permissible ω-k_x regions within the light lines highlighted. Waves incident from the homogeneous medium at all angles, and both polarizations, are represented by points within this region; points outside this region are not accessible by waves incident from the homogeneous medium regardless of their angle of incidence or polarization. The spectral band bounded by the angular frequencies ω_1 and ω_2, as defined in Fig. 7.2-10, is of particular interest inasmuch as all ω-k_x points lying in this band are within a photonic bandgap. In this spectral band, therefore, no incident wave, regardless of its angle or polarization, can be matched with a propagating wave in the periodic medium — the boundary then acts as a perfect omnidirectional reflector. Also illustrated in Fig. 7.2-10 is a second spectral band, at higher angular frequencies, that behaves in the same way.

Slab of Periodic Material in a Homogeneous Medium

A slab of 1D periodic material embedded in a homogeneous medium is nothing but a 1D Bragg grating with a finite number of segments. Reflection and transmission from the Bragg grating has already been examined in Sec. 7.1C.

One would expect that a Bragg grating with a large, but finite, number of segments N captures the basic properties of a periodic medium made of the same unit cell. This is in fact the case since the passbands and stop bands of the grating are mathematically identical to the photonic bands and bandgaps of the extended periodic medium. However, the spectral transmittance and reflectance of the Bragg grating, which exhibit oscillatory properties sensitive to the size of the grating and the presence of its boundaries, do not have their counterparts in the extended periodic structure.
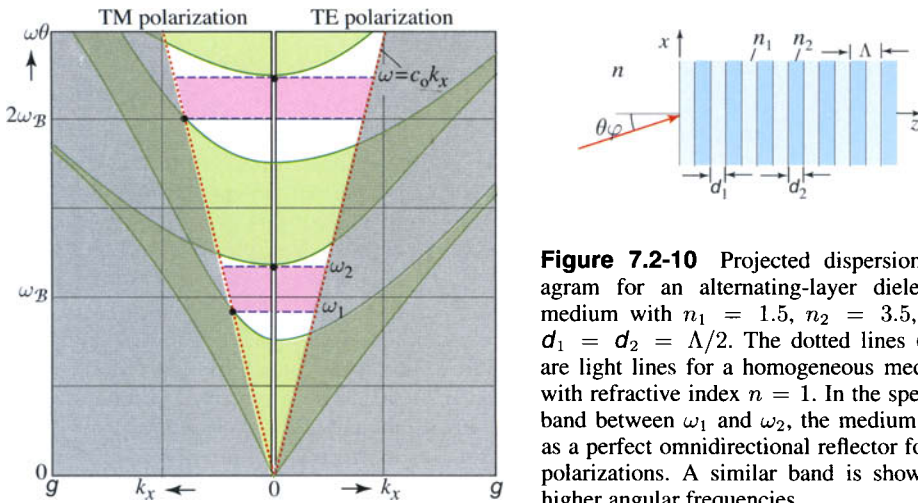
Figure 7.2-10 Projected dispersion diagram for an alternating-layer dielectric medium with $n_1 = 1.5$, $n_2 = 3.5$, and $d_1 = d_2 = \Lambda/2$. The dotted lines (red) are light lines for a homogeneous medium with refractive index $n = 1$. In the spectral band between ω_1 and ω_2, the medium acts as a perfect omnidirectional reflector for all polarizations. A similar band is shown at higher angular frequencies.

Likewise, the phase and group velocities and the associated effective refractive indexes determined from the dispersion relation in the extended periodic medium do not have direct counterparts in the finite-size Bragg grating. Nevertheless, such parameters can be defined for a grating by determining the complex amplitude transmittance $t(\omega)$ and matching it with an effective homogeneous medium of the same total thickness d such that $\arg\{t_N\} = (\omega/c_o)n_{\text{eff}}d$. An effective group index $N_{\text{eff}} = n_{\text{eff}} + \omega dn_{\text{eff}}/d\omega$ is then determined [see (5.6-2)]. The dependence of these effective indexes on frequency is different from that shown in Fig. 7.2-6 for the extended periodic medium in that it exhibits oscillations within the passbands. However, for sufficiently large N, say greater than 100, these oscillations are washed out and the effective indexes become nearly the same as those of the extended periodic medium.

Another configuration of interest is a slab of homogeneous medium embedded in a periodic medium. In this configuration, the light may be trapped in the slab by omnidirectional reflection from the surrounding periodic medium, so that the slab becomes an optical waveguide. This configuration is discussed in Sec. 8.4.

7.3 TWO- AND THREE-DIMENSIONAL PHOTONIC CRYSTALS

The concepts introduced in Sec. 7.2 for the study of optical-wave propagation in 1D periodic media can be readily generalized to 2D and 3D structures. These include Bloch waves as the modes of the periodic medium and ω-K dispersion relations with photonic bands and bandgaps. In contrast to 1D structures, 2D photonic crystals have 2D-complete photonic bandgaps, i.e., common bandgaps for waves of both polarization traveling in any direction in the plane of periodicity. However, 3D-complete photonic bandgaps, i.e., common bandgaps for all directions and polarizations, can be achieved only in 3D photonic crystals. The mathematical treatment of 2D and 3D periodic media is more elaborate and the visualization of the dispersion diagrams is more difficult because of the additional degrees of freedom involved, but the concepts are essentially the same as those encountered for 1D periodic media. This section begins with a simple treatment of 2D structures followed by a more detailed 3D treatment.

A. Two-Dimensional Photonic Crystals

2D Periodic Structures

Consider a 2D periodic structure such as a set of identical parallel rods, tubes, or veins embedded in a homogeneous host medium [Fig. 7.3-1(a)] and organized at the points of a rectangular lattice, as illustrated in Fig. 7.3-1(b). The impermeability $\eta(x,y) = \epsilon_o/\epsilon(x,y)$ is periodic in the transverse directions, x and y, and uniform in the axial direction z. If a_1 and a_2 are the periods in the x and y directions, then $\eta(x,y)$ satisfies the translational symmetry relation

$$\eta(x + m_1 a_1, y + m_2 a_2) = \eta(x,y), \tag{7.3-1}$$

for all integers m_1 and m_2. This periodic function is represented as a 2D Fourier series,

$$\eta(x,y) = \sum_{\ell_1=-\infty}^{\infty} \sum_{\ell_2=-\infty}^{\infty} \eta_{\ell_1,\ell_2} \exp\left(-j\ell_1 \boldsymbol{g}_1 x\right) \exp\left(-j\ell_2 \boldsymbol{g}_2 x\right), \tag{7.3-2}$$

where $\boldsymbol{g}_1 = 2\pi/a_1$ and $\boldsymbol{g}_2 = 2\pi/a_2$ are fundamental spatial frequencies (radians/mm) in the x and y directions, and $\ell_1 \boldsymbol{g}_1$ and $\ell_2 \boldsymbol{g}_2$ are their harmonics. The coefficients η_{ℓ_1,ℓ_2} depend on the actual profile of the periodic function, e.g., the size of the rods.

The 2D Fourier transform of the periodic function is composed of points (delta functions) on a rectilinear lattice, as shown in Fig. 7.3-1(c). This Fourier-domain lattice is known to solid-state physicists as the **reciprocal lattice**.

What are the optical modes of a medium with such symmetry? The answer is a simple generalization of the 1D case given in (7.2-4). For waves traveling in a direction parallel to the x–y plane, the modes are 2D Bloch waves,

$$U(x,y) = p_{K_x,K_y}(x,y) \exp(-jK_x x)\exp(-jK_y y), \tag{7.3-3}$$

where $p_{K_x,K_y}(x,y)$ is a periodic function with the same periods as the medium. The wave is specified by a pair of Bloch wavenumbers (K_x, K_y). Another wave with Bloch wavenumbers $(K_x + \boldsymbol{g}_1, K_y + \boldsymbol{g}_2)$ is not a new mode. As shown in Fig. 7.3-1(c) a complete set of modes in the Fourier plane has Bloch wavenumbers located at points in a rectangle defined by $[-\boldsymbol{g}_1/2 < K_x \leqslant \boldsymbol{g}_1/2]$ and $[-\boldsymbol{g}_2/2 < K_y \leqslant \boldsymbol{g}_2/2]$, which is the first Brillouin zone.

Other symmetries may be used to reduce the set of independent Bloch wavevectors within the Brillouin zone. When all symmetries are included, the result is an area called the **irreducible Brillouin zone**. For example, the rotational symmetry inherent in the square lattice results in an irreducible Brillouin zone in the form of a triangle, as shown in Fig 7.3-1(d).

2D Skew-Periodic Structures

An example of another class of 2D periodic structures is a set of parallel cylindrical holes placed at the points of a triangular lattice, as illustrated in Fig. 7.3-2(a). Since the lattice points are skewed (not aligned with x and y axis), we use two primitive *vectors* $\mathbf{a}_1$ and $\mathbf{a}_2$ [Fig. 7.3-2(b)] to generate the lattice via the lattice vector $\mathbf{R} = m_1\mathbf{a}_1 + m_2\mathbf{a}_2$, where m_1 and m_2 are integers. We also define a position vector $\mathbf{r}_T = (x,y)$ so that the periodic function $\epsilon(\mathbf{r}_T) \equiv \epsilon(x,y)$ satisfies the translational symmetry relation $\epsilon(\mathbf{r}_T + \mathbf{R}) = \epsilon(\mathbf{r}_T)$ (the subscript "T" indicates transverse).

The 2D Fourier series of such a function is a set of points on a reciprocal lattice defined by the vectors $\mathbf{g}_1$ and $\mathbf{g}_2$, which are orthogonal to $\mathbf{a}_1$ and $\mathbf{a}_2$, respectively, and have magnitudes $\boldsymbol{g}_1 = 2\pi/a_1 \sin\theta$ and $\boldsymbol{g}_2 = 2\pi/a_2 \sin\theta$, where θ is the angle between $\mathbf{a}_1$ and $\mathbf{a}_2$. The 2D reciprocal lattice is also a triangular lattice generated by

(a) 2D periodic structure   *(b)* Lattice   *(c)* Reciprocal lattice   *(d)* Irreducible Brillouin zone
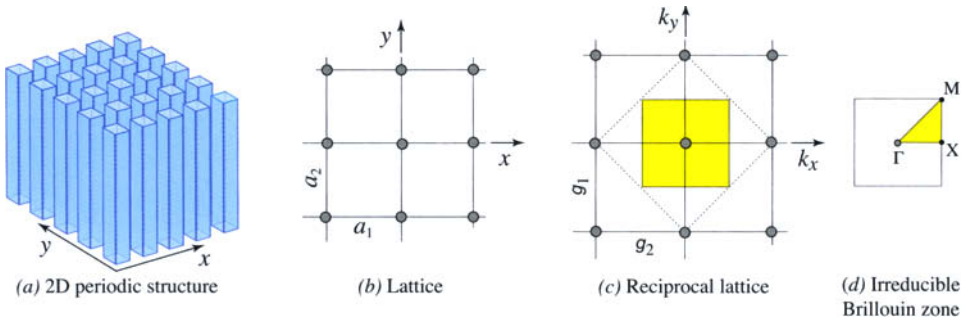
Figure 7.3-1   *(a)* A 2D periodic structure comprising parallel rods. *(b)* The rectangular lattice at which the rods are placed. *(c)* The 2D Fourier transform of the lattice points is another set of points forming a reciprocal lattice with periods $g_1 = 2\pi/a_1$ and $g_2 = 2\pi/a_2$. The shaded (yellow) area is the Brillouin zone. *(d)* For a square lattice ($a_1 = a_2 = a$), the irreducible Brillouin zone is the triangle ΓMX.
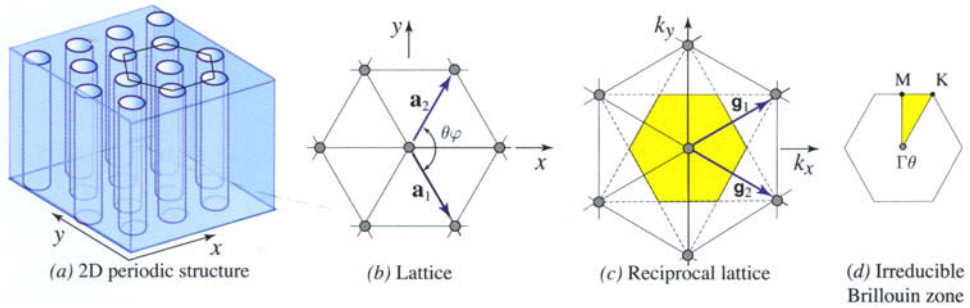

(a) 2D periodic structure   *(b)* Lattice   *(c)* Reciprocal lattice   *(d)* Irreducible Brillouin zone

Figure 7.3-2   *(a)* A 2D periodic structure comprising parallel cylindrical holes. *(b)* The triangular lattice at which the holes are placed. In this diagram the magnitudes $a_1 = a_2 = a$ and $\theta = 120°$. *(c)* Reciprocal lattice; the shaded (yellow) area is the Brillouin zone, a hexagon. *(d)* The irreducible Brillouin zone is the triangle ΓMK.

the vector $\mathbf{G} = \ell_1\mathbf{g}_1 + \ell_2\mathbf{g}_2$, where ℓ_1 and ℓ_2 are integers, as illustrated in Fig. 7.3-2(*c*).

For waves traveling in a direction parallel to the x–y plane, the Bloch modes are

$$U(\mathbf{r}_{\mathrm{T}}) = p_{\mathbf{K}}(\mathbf{r}_{\mathrm{T}}) \exp(-j\mathbf{K}_{\mathrm{T}} \cdot \mathbf{r}_{\mathrm{T}}), \qquad (7.3\text{-}4)$$

where $\mathbf{K}_{\mathrm{T}} = (K_x, K_y)$ is the Bloch wavevector and $p_{\mathbf{K}_{\mathrm{T}}}(\mathbf{r}_{\mathrm{T}})$ is a 2D periodic function on the same lattice. Two Bloch modes with Bloch wavevectors $\mathbf{K}_{\mathrm{T}}$ and $\mathbf{K}_{\mathrm{T}} + \mathbf{G}$ are equivalent. To cover a complete set of Bloch wavevectors, we therefore need only consider vectors within the Brillouin zone shown in Fig. 7.3-2(*c*).

The dispersion relation can be determined by ensuring that the Bloch wave in (7.3-3) or (7.3-4) satisfies the generalized Helmholtz equation. The calculations are facilitated by use of a Fourier series approach, as was done in the 1D case and as will be described (in a more general form) in the 3D case.

EXAMPLE 7.3-1.   *Cylindrical Holes on a Triangular Lattice.*   A 2D photonic crystal comprises a homogeneous medium ($n = 3.6$) with air-filled cylindrical holes of radius $0.48a$ organized at the points of a triangular lattice with lattice constant a. The calculated dispersion relation, shown in Fig. 7.3-3, for TE and TM waves traveling in the plane of periodicity ($k_z = 0$) exhibits a 2D-complete

photonic bandgap at frequencies near the angular frequency $\omega_0 = \pi c_o/a$.[†] As in the 1D case, the gap can be made wider by use of materials with greater refractive-index contrast. Indeed, most geometries exhibit photonic bandgaps if the materials used have sufficiently high contrast.
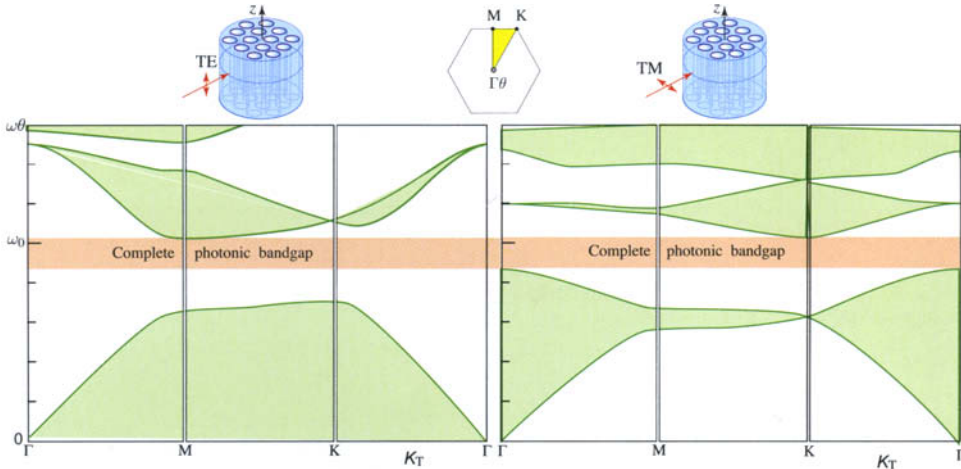

Figure 7.3-3   Calculated band structure of a 2D photonic crystal made of a homogeneous medium ($n = 3.6$) with air-filled cylindrical holes of radius $0.48a$ organized at the points of a triangular lattice with lattice constant a. The abscissa spans Bloch wavevectors defined by points on the periphery of the irreducible Brillouin zone, the ΓMK triangle. The ordinate is plotted in units of $\omega_0 = \pi c_o/a$. The wave travels in the plane of periodicity and has TE polarization (left) and TM polarization (right).

This photonic-crystal structure finds use as a "holey" optical fiber, which has a number of salutary properties (see Sec. 9.4).

For an oblique wave traveling at an angle with respect to the x–y plane, the Bloch wave in (7.3-4) becomes

$$U(\mathbf{r}_{\mathrm{T}}) = p_{\mathbf{\kappa}}(\mathbf{r}_{\mathrm{T}}) \exp(-j\mathbf{K}_{\mathrm{T}} \cdot \mathbf{r}_{\mathrm{T}}) \exp(-jk_z z), \qquad (7.3-5)$$

where k_z is a constant. The band structure then takes the form of a set of surfaces of $\omega = \omega(\mathbf{K}_{\mathrm{T}}, k_z)$.

A 3D-complete photonic bandgap is a range of frequencies ω crossed by none of these surfaces, i.e., values of ω that are not obtained by any combination of real $\mathbf{K}_{\mathrm{T}}$ and k_z. While a 2D-complete photonic bandgap exists for $k_z = 0$, as illustrated by the example in Fig. 7.3-3, a photonic bandgap for all off-axis waves is not attainable in 2D periodic structures.

B. Three-Dimensional Photonic Crystals

Crystal Structure

A 3D photonic crystal is generated by placement of duplicates of a basic dielectric structure, such as a sphere or a cube, at points of a 3D lattice generated by the lattice vectors $\mathbf{R} = m_1\mathbf{a}_1 + m_2\mathbf{a}_2 + m_3\mathbf{a}_3$, where m_1, m_2, and m_3 are integers, and $\mathbf{a}_1$, $\mathbf{a}_2$, and

---

[†] See S. G. Johnson and J. D. Joannopoulos, Block-Iterative Frequency-Domain Methods for Maxwell's Equations in a Planewave Basis, *Optics Express*, vol. 8, pp. 173–190, 2001.

$\mathbf{a}_3$ are primitive vectors defining the lattice unit cell. The overall structure is periodic and its physical properties, such as the permittivity $\epsilon(\mathbf{r})$ and the impermeability $\eta(\mathbf{r}) = \epsilon_o/\epsilon(\mathbf{r})$, are invariant to translation by $\mathbf{R}$, e.g.,

$$\eta(\mathbf{r} + \mathbf{R}) = \eta(\mathbf{r}), \qquad (7.3\text{-}6)$$

for all positions $\mathbf{r}$. This periodic functions may therefore be expanded in a 3D Fourier series,

$$\eta(\mathbf{r}) = \sum_{\mathbf{G}} \eta_{\mathbf{G}} \exp(-j\,\mathbf{G}\cdot\mathbf{r}), \qquad (7.3\text{-}7)$$

where $\mathbf{G} = \ell_1\mathbf{g}_1 + \ell_2\mathbf{g}_2 + \ell_3\mathbf{g}_3$ is a vector defined by the primitive vectors $\mathbf{g}_1$, $\mathbf{g}_2$, and $\mathbf{g}_3$ of another lattice, the **reciprocal lattice**, and ℓ_1, ℓ_2, and ℓ_3, are integers. The $\mathbf{g}$ vectors are related to the $\mathbf{a}$ vectors via

$$\mathbf{g}_1 = 2\pi\frac{\mathbf{a}_2 \times \mathbf{a}_3}{\mathbf{a}_1 \cdot \mathbf{a}_2 \times \mathbf{a}_3}, \quad \mathbf{g}_2 = 2\pi\frac{\mathbf{a}_3 \times \mathbf{a}_1}{\mathbf{a}_1 \cdot \mathbf{a}_2 \times \mathbf{a}_3}, \quad \mathbf{g}_3 = 2\pi\frac{\mathbf{a}_1 \times \mathbf{a}_2}{\mathbf{a}_1 \cdot \mathbf{a}_2 \times \mathbf{a}_3}, \quad (7.3\text{-}8)$$

so that $\mathbf{g}_1 \cdot \mathbf{a}_1 = 2\pi$, $\mathbf{g}_1 \cdot \mathbf{a}_2 = 0$, and $\mathbf{g}_1 \cdot \mathbf{a}_3 = 0$, i.e., $\mathbf{g}_1$ is orthogonal to $\mathbf{a}_2$ and $\mathbf{a}_3$ and its length is inversely proportional to $\mathbf{a}_1$. Similar properties apply to $\mathbf{g}_2$ and $\mathbf{g}_3$. It can also be shown that $\mathbf{G} \cdot \mathbf{R} = 2\pi$.

If $\mathbf{a}_1$, $\mathbf{a}_2$, and $\mathbf{a}_3$ are mutually orthogonal, then $\mathbf{g}_1$, $\mathbf{g}_2$, and $\mathbf{g}_3$ are also mutually orthogonal and the magnitudes $g_1 = 2\pi/a_1$, $g_2 = 2\pi/a_2$, and $g_3 = 2\pi/a_3$ are the spatial frequencies associated with the periodicities in the three directions, respectively. An example of a 3D crystal lattice and its corresponding reciprocal lattice is shown in Fig. 7.3-4.
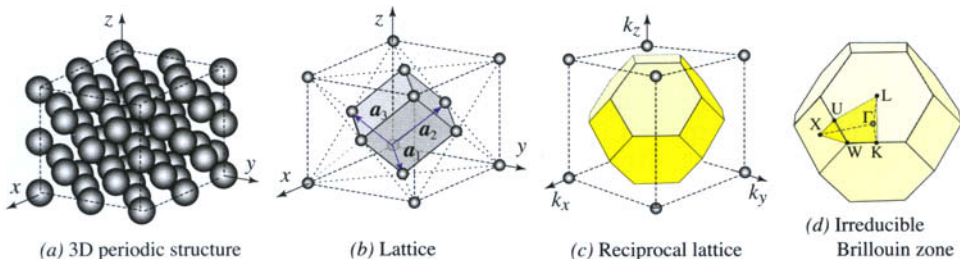

(a) 3D periodic structure   (b) Lattice   (c) Reciprocal lattice   (d) Irreducible Brillouin zone

Figure 7.3-4 (a) A 3D periodic structure comprising dielectric spheres. (b) The spheres are placed at the points of a diamond (face-centered cubic) lattice for which $\mathbf{a}_1 = (a/\sqrt{2})(\hat{\mathbf{x}} + \hat{\mathbf{y}})$, $\mathbf{a}_2 = (a/\sqrt{2})(\hat{\mathbf{y}}+\hat{\mathbf{z}})$, and $\mathbf{a}_3 = (a/\sqrt{2})(\hat{\mathbf{x}}+\hat{\mathbf{z}})$, where a is the lattice constant. (c) The corresponding reciprocal lattice is a body-centered cubic lattice with a Brillouin zone indicated by the shaded volume, known as a Wigner–Seitz cell. (d) The irreducible Brillouin zone is the polyhedron whose corner points are marked by the crystallographic symbols $\Gamma\mathrm{XULKW}$.

Bloch Modes

The modes of a 3D periodic medium are waves that maintain their shape upon translation by a lattice vector $\mathbf{R}$, changing only by a multiplicative constant of unity magnitude. These modes have the Bloch form $p_{\mathbf{K}}(\mathbf{r}) \exp(-j\mathbf{K}\cdot\mathbf{r})$ where $p_{\mathbf{K}}(\mathbf{r})$ is a 3D periodic function, with the periodicity described by the same lattice vector $\mathbf{R}$; $\mathbf{K}$ is the **Bloch wavevector**; and $\hat{\mathbf{e}}$ is a unit vector in the direction of polarization. The Bloch mode is a traveling plane wave $\exp(-j\mathbf{K}\cdot\mathbf{r})$ modulated by a periodic function $p_{\mathbf{K}}(\mathbf{r})$.

Translation by **R** results in multiplication by a phase factor $\exp(-j\mathbf{K} \cdot \mathbf{R})$, which depends on **K**.

Two modes with Bloch wavevectors **K** and $\mathbf{K}' = \mathbf{K} + \mathbf{G}$ are equivalent since $\exp(-j\mathbf{K}' \cdot \mathbf{R}) = \exp(-j\mathbf{K} \cdot \mathbf{R})$, i.e., translation by **R** is equivalent to multiplication by the same phase factor. This is because $\exp(-j\mathbf{G} \cdot \mathbf{R}) = \exp(-j2\pi) = 1$. Therefore, for the complete specification of all modes, we need only consider values of **K** within a finite volume of the reciprocal lattice, the Brillouin zone. The Brillouin zone is the volume of points that are closer to one specific reciprocal lattice point (the origin of the zone, denoted Γ) than to any other lattice point. Other symmetries of the lattice permit further reduction of that volume to the irreducible Brillouin zone, as illustrated by the example in Fig. 7.3-4.

Photonic Band Structure

To determine the ω–**K** dispersion relation for a 3D periodic medium, we begin with the eigenvalue problem described by the generalized Helmholtz equation (7.0-2). One approach for solving this problem is to generalize the Fourier method that was introduced in Sec. 7.2C for 1D periodic structures. By expanding the periodic functions $\eta(\mathbf{r})$ and $p_\mathbf{K}(\mathbf{r})$ in Fourier series, the differential equation (7.0-2) is converted into a set of algebraic equations leading to a matrix eigenvalue problem that can be solved numerically using matrix methods. As discussed at the end of Sec. 7.2C, we work with the magnetic field to ensure Hermiticity of the matrix representation.

Expanding the periodic function $p_\mathbf{K}(\mathbf{r})$ in the Bloch wave into a 3D Fourier series

$$p_\mathbf{K}(\mathbf{r}) = \sum_\mathbf{G} C_\mathbf{G} \exp(-j\,\mathbf{G} \cdot \mathbf{r}), \tag{7.3-9}$$

we write the magnetic field vector in the Bloch form

$$\mathbf{H}(\mathbf{r}) = p_\mathbf{K}(\mathbf{r}) \exp(-j\mathbf{K} \cdot \mathbf{r})\widehat{e} = \sum_\mathbf{G} C_\mathbf{G} \exp[-j(\mathbf{K} + \mathbf{G}) \cdot \mathbf{r}]\widehat{e}. \tag{7.3-10}$$

For notational simplicity, the dependence of the Fourier coefficients $C_\mathbf{G}$ on the Bloch wavevector **K** is not explicitly indicated. Substituting (7.3-7) and (7.3-10) into (7.0-2), using the relation $\nabla \times \exp(-j\mathbf{K} \cdot \mathbf{r})\,\widehat{e} = -j(\mathbf{K} \times \widehat{e})\exp(-j\mathbf{K} \cdot \mathbf{r})$, and equating harmonic terms of the same spatial frequency yields

$$-\sum_{\mathbf{G}'} (\mathbf{K} + \mathbf{G}) \times \left[(\mathbf{K} + \mathbf{G}') \times \widehat{e}\right] \eta_{\mathbf{G}-\mathbf{G}'} C_{\mathbf{G}'} = \frac{\omega^2}{c_o^2} C_\mathbf{G}\,\widehat{e}. \tag{7.3-11}$$

Forming a dot product with $\widehat{e}$ on both sides, and using the vector identity $\mathbf{A} \cdot (\mathbf{B} \times \mathbf{C}) = -(\mathbf{B} \times \mathbf{A}) \cdot \mathbf{C}$ leads to

$$\sum_{\mathbf{G}'} F_{\mathbf{G}\mathbf{G}'} C_{\mathbf{G}'} = \frac{\omega^2}{c_o^2} C_\mathbf{G}\,, \quad F_{\mathbf{G}\mathbf{G}'} = \left[(\mathbf{K}+\mathbf{G}) \times \widehat{e}\right] \cdot \left[(\mathbf{K}+\mathbf{G}') \times \widehat{e}\right] \eta_{\mathbf{G}-\mathbf{G}'}. \tag{7.3-12}$$

The Helmholtz differential equation has now been converted into a set of linear equations for the Fourier coefficients $\{C_\mathbf{G}\}$. Since $\eta(z)$ is real, $\eta_{\mathbf{G}-\mathbf{G}'} = \eta_{\mathbf{G}'-\mathbf{G}}^*$, and the matrix $F_{\mathbf{G}\mathbf{G}'}$ is Hermitian. Hence, (7.3-12) represents an eigenvalue problem for a Hermitian matrix. For each Bloch wavevector **K**, the eigenvalues ω^2/c_o^2 provide multiple values of ω, which are used to construct the ω-**K** diagram and the photonic band structure. The eigenvectors $\{C_\mathbf{G}\}$ determine the periodic function $p_\mathbf{K}(\mathbf{r})$ of the Bloch wave.

Examples

Spherical holes on a diamond lattice. An example of a 3D photonic crystal that has been shown to exhibit a complete 3D photonic bandgap comprises air spheres embedded in a high-index material at the points of a diamond lattice (see Fig. 7.3-4). The radius of the air spheres is sufficiently large so that the spheres overlap, thereby creating intersecting veins. The calculated band structure shown in Fig. 7.3-5 has a relatively wide complete 3D photonic bandgap between the two lowest bands.[†] Photonic crystals using spherical holes in silicon have been fabricated by growing silicon inside the voids of an opal template of close-packed silica spheres that are connected by small "necks" formed during sintering, followed by removal of the silica template.[‡]
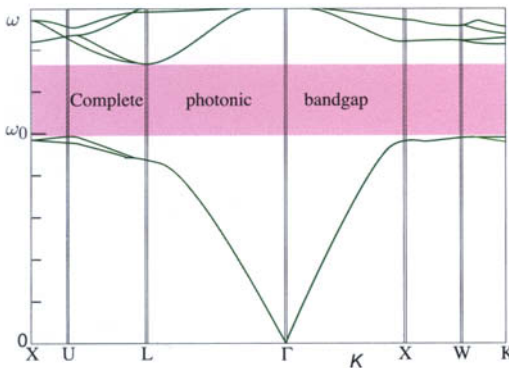

Figure 7.3-5 Calculated band structure of a 3D photonic crystal with a diamond lattice of lattice constant a. The structure comprises air spheres of radius $0.325\,a$ embedded in a homogeneous material of refractive index $n = 3.6$. The gap extends from approximately $\omega_0 = \pi c_o/a$ to $1.32\,\omega_0$.

Yablonovite. The first experimental observation of a 3D complete photonic bandgap was made by Eli Yablonovitch in 1991 using a variant of the diamond lattice structure, now known as the **Yablonovite**. This slanted-pore structure is fabricated by drilling a periodic array of cylindrical holes at specified angles in a dielectric slab. Three holes are drilled at each point of a 2D triangular lattice at the surface of the slab; the directions of the holes are parallel to three of the axes of the diamond lattice, as shown in Fig. 7.3-6(a). This structure has a complete gap with a gap-midgap ratio of 0.19 when the refractive index is $n = 3.6$.

Woodpile. Another 3D photonic-crystal structure, which is simpler to fabricate, is made of a 1D periodic stack of alternating layers, each of which is itself a 2D photonic crystal. For example, the woodpile structure illustrated in Fig. 7.3-6(b) uses layers of parallel logs with a stacking sequence that repeats itself every four layers. The orientation of the logs in adjacent layers is rotated 90°, and the logs are shifted by half the pitch every two layers. The resulting structure has a face-centered-tetragonal lattice symmetry. Fabricated using silicon technology, at a minimum feature size of 180 nm this structure manifested a complete 3D photonic bandgap in the wavelength range $\lambda = 1.35$–$1.95\ \mu\text{m}$.[*]

[†] See S. G. Johnson and J. D. Joannopoulos, Block-Iterative Frequency-Domain Methods for Maxwell's Equations in a Planewave Basis, *Optics Express*, vol. 8, pp. 173–190, 2001.

[‡] See A. Blanco *et al.*, Large-Scale Synthesis of a Silicon Photonic Crystal with a Complete Three-dimensional Bandgap Near 1.5 Micrometres, *Nature*, vol. 405, pp. 437–440, 2000.

[*] See J. G. Fleming and S.-Y. Lin, Three-Dimensional Photonic Crystal with a Stop Band from 1.35 to 1.95 μm, *Optics Letters*, vol. 24, pp. 49–51, 1999.

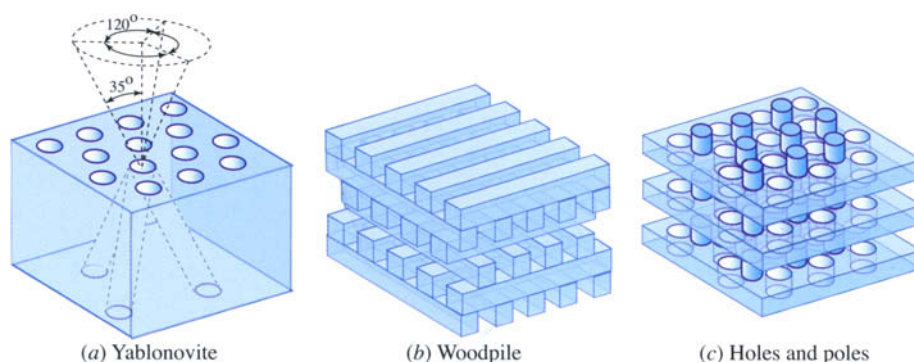(a) Yablonovite   (b) Woodpile   (c) Holes and poles

Figure 7.3-6 (a) The Yablonovite photonic crystal is fabricated by drilling cylindrical holes through a dielectric slab. At each point of a 2D triangular lattice at the surface, three holes are drilled along directions that make an angle of 35° with the normal and are separated azimuthally by 120°. (b) The woodpile photonic crystal comprises alternating layers of parallel rods, with adjacent layers oriented at 90°. (c) The holes-and-poles structure is made of alternating layers of 2D periodic structures: a layer of parallel cylindrical holes on a hexagonal lattice, followed by a layer of parallel rods lined up to fit between the holes.

Holes and poles. Yet another example is the holes-and-poles structure illustrated in Fig. 7.3-6(c). Here, two complementary types of 2D-periodic photonic-crystal slabs are used: dielectric rods in air and air holes in a dielectric. Fabricated in silicon, this structure exhibited a stop-band for all tilt angles in the wavelength range $\lambda = 1.15$–1.6 μm [†]

Both the holes-and-poles structure and the woodpile structure offer the opportunity of introducing arbitrary **point defects**, such as a missing hole or rod, which provide means for fabricating devices such as photonic crystal waveguides (see Sec. 8.5), photonic-crystal nano-resonators (see Sec. 10.4D), and specially controlled light emitters[‡] (see Chapter 17). Indeed, the ability to insert a defect at will is the most valuable feature of 2D and 3D photonic structures since 1D periodic media serve admirably as omnidirectional reflectors.

READING LIST

Books on Layered and Periodic Media

Š. Višňovský, *Optics in Magnetic Multilayers and Nanostructures*, CRC Press, 2006.

O. Stenzel, *The Physics of Thin Film Optical Spectra: An Introduction*, Springer-Verlag, 2005.

P. Yeh, *Optical Waves in Layered Media*, Wiley, 2005.

L. Brillouin, *Wave Propagation in Periodic Structures: Electric Filters and Crystal Lattices*, Dover, 2nd ed. 1953, reprinted 2003.

M. Nevière and E. Popov, *Light Propagation in Periodic Media: Differential Theory and Design*, Marcel Dekker, 2003.

M. Born and E. Wolf, *Principles of Optics*, Cambridge University Press, 7th expanded and corrected ed. 2002, Sec. 1.6.

R. Kashyap, *Fiber Bragg Gratings*, Academic Press, 1999.

W. C. Chew, *Waves and Fields in Inhomogeneous Media*, Van Nostrand Reinhold, 1990.

A. Yariv and P. Yeh, *Optical Waves in Crystals: Propagation and Control of Laser Radiation*, Wiley, 1985.

[†] See M. Qi, E. Lidorikis, P. T. Rakich, S. G. Johnson, J. D. Joannopoulos, E. P. Ippen, and H. I. Smith, A Three-Dimensional Optical Photonic Crystal with Designed Point Defects, *Nature*, vol. 429, pp. 538–542, 2004.

[‡] See S. P. Ogawa, M. Imada, S. Yoshimoto, M. Okano, and S. Noda, Control of Light Emission by 3D Photonic Crystals, *Science*, vol. 305, pp. 227–229, 2004.

Books on Photonic Crystals

J. D. Joannopoulos, S. G. Johnson, J. N. Winn, and R. D. Meade, *Photonic Crystals: Molding the Flow of Light*, Princeton University Press, 1995, 2nd ed. 2008.

P. Markoš and C. M. Soukoulis, *Wave Propagation: From Electrons to Photonic Crystals and Left-Handed Materials*, Princeton University Press, 2008.

K. Yasumoto, ed., *Electromagnetic Theory and Applications for Photonic Crystals*, CRC Press, 2006.

J.-M. Lourtioz, H. Benisty, V. Berger, J.-M. Gérard, D. Maystre, and A. Tchelnokov, *Photonic Crystals: Towards Nanoscale Photonic Devices*, Springer-Verlag, 2005.

K. Sakoda, *Optical Properties of Photonic Crystals*, Springer-Verlag, 2nd ed. 2005.

K. Busch, S. Lölkes, R. B. Wehrspohn, and H. Föll, eds., *Photonic Crystals: Advances in Design, Fabrication, and Characterization*, Wiley, 2004.

K. Inoue and K. Ohtaka, eds., *Photonic Crystals: Physics, Fabrication and Applications*, Springer-Verlag, 2004.

S. Noda and T. Baba, eds., *Roadmap on Photonic Crystals*, Kluwer, 2003.

V. Kochergin, *Omnidirectional Optical Filters*, Kluwer, 2003.

R. E. Slusher and B. J. Eggleton, eds., *Nonlinear Photonic Crystals*, Springer-Verlag, 2003.

S. G. Johnson and J. D. Joannopoulos, *Photonic Crystals: The Road from Theory to Practice*, Springer-Verlag, 2002.

M. Senechal, *Quasicrystals and Geometry*, Cambridge University Press, 1995.

Articles

Issue on nanophotonics, *IEEE Journal of Selected Topics in Quantum Electronics*, vol. 12, no. 6, 2006.

A. Adibi, S.-Y. Lin, and A. Scherer, eds., Photonic crystal materials and devices III, *SPIE Proceedings*, vol. 5733, 2005.

A. Adibi, A. Scherer, and S.-Y. Lin, eds., Photonic crystal materials and devices II, *SPIE Proceedings*, vol. 5360, 2004.

S. P. Ogawa, M. Imada, S. Yoshimoto, M. Okano, and S. Noda, Control of Light Emission by 3D Photonic Crystals, *Science*, vol. 305, pp. 227–229, 2004.

M. Qi, E. Lidorikis, P. T. Rakich, S. G. Johnson, J. D. Joannopoulos, E. P. Ippen, and H. I. Smith, A Three-Dimensional Optical Photonic Crystal with Designed Point Defects, *Nature*, vol. 429, pp. 538–542, 2004.

A. Adibi, A. Scherer, and S.-Y. Lin, eds., Photonic crystal materials and devices I, *SPIE Proceedings*, vol. 5000, 2003.

E. Yablonovitch, Photonic Crystals: Semiconductors of Light, *Scientific American*, vol. 285, no. 6, pp. 47–55, 2001.

M. Deopura, C. K. Ullal, B. Temelkuran, and Y. Fink, Dielectric Omnidirectional Visible Reflector, *Optics Letters*, vol. 26, pp. 1197–1199, 2001.

Focus issue on photonic bandgap calculations, *Optics Express*, vol. 8, no. 3, 2001.

S. G. Johnson and J. D. Joannopoulos, Block-Iterative Frequency-Domain Methods for Maxwell's Equations in a Planewave Basis, *Optics Express*, vol. 8, pp. 173–190, 2001.

M. Müller, R. Zentel, T. Maka, S. G. Romanov, and C. M. Sotomayor Torres, Photonic Crystal Films with High Refractive Index Contrast, *Advanced Materials*, vol. 12, pp. 1499–1503, 2000.

A. Blanco, E. Chomski, S. Grabtchak, M. Ibisate, S. John, S. W. Leonard, C. Lopez, F. Meseguer, H. Miguez, J. P. Mondia, G. A. Ozin, O. Toader, and H. M. van Driel, Large-Scale Synthesis of a Silicon Photonic Crystal with a Complete Three-dimensional Bandgap Near 1.5 Micrometres, *Nature*, vol. 405, pp. 437–440, 2000.

Y. Fink, J. N. Winn, S. Fan, C. Chen, J. Michel, J. D. Joannopoulos, and E. L. Thomas, A Dielectric Omnidirectional Reflector, *Science*, vol. 282, pp. 1679–1682, 1998.

J. M. Bendickson, J. P. Dowling, and M. Scalora, Analytic Expressions for the Electromagnetic Mode Density in Finite, One-Dimensional, Photonic Band-Gap Structures, *Physical Review E*, vol. 53, pp. 4107–4121, 1996.

P. R. Villeneuve and M. Piché, Photonic Bandgaps in Periodic Dielectric Structures, *Progress in Quantum Electronics*, vol. 18, pp. 153–200, 1994.

S. John, Localization of Light, *Physics Today*, vol. 44, no. 5, pp. 32–40, 1991.

E. Yablonovitch, T. J. Gmitter, and K. M. Leung, Photonic Band Structures: The Face-Centered Cubic Case Employing Non-Spherical Atoms, *Physical Review Letters*, vol. 67, pp. 2295–2298, 1991.

E. Yablonovitch and T. J. Gmitter, Photonic Band Structure: The Face-Centered-Cubic Case, *Journal of the Optical Society of America A*, vol. 7, pp. 1792–1800, 1990.

S. John, Strong Localization of Photons in Certain Disordered Dielectric Superlattices, *Physical Review Letters*, vol. 58, pp. 2486–2489, 1987.

E. Yablonovitch, Inhibited Spontaneous Emission in Solid-State Physics and Electronics, *Physical Review Letters*, vol. 58, pp. 2059–2062, 1987.

PROBLEMS

7.1-2   Beamsplitter Slab. A dielectric lossless slab of refractive index n and width d, oriented at $45°$ with respect to an incident beam, is used as a beamsplitter. Derive expressions for the transmittance and reflectance and sketch their spectral dependence for TE and TM polarization.

7.1-3   Air Gap in Glass. Determine the transmittance through a thin planar air gap of width $d = \lambda/2$ in glass of refractive index n. Assume (a) normal incidence, and (b) a TE wave incident at an angle greater than the critical angle. Can the wave penetrate (tunnel) through the gap?

7.1-4   Multilayer Device in an Unmatched Medium. The complex amplitude reflectance of a multilayer device is r_m when it is placed in a medium with refractive index n_1 matching its front layer. If the device is instead placed in a medium with refractive index n, show that the amplitude reflectance is $r = (r_b + r_m)/(1 + r_b r_m)$, where $r_b = (n - n_1)/(n + n_1)$ is the reflectance of the new boundary. Determine r in each of the following limiting cases: $r_b = 0$, $r_b = 1$, $r_m = 0$, and $r_m = 1$.

7.1-5   Quarter-Wave Film: Angular Dependence of Reflectance. Consider the quarter-wave antireflection coating described in Exercise 7.1-1. Derive an expression for the reflectance as a function of the angle of incidence.

7.1-6   Quarter-Wave and Half-Wave Stacks. Derive expressions for the reflectance of a stack of N double layers of dielectric materials of equal optical thickness, $n_1 d_1 = n_2 d_2$, equal to $\lambda_o/4$ and $\lambda_o/2$.

7.1-7   GaAs/AlAs Bragg Grating Reflector. A Bragg grating reflector comprises N units of alternating layers of GaAs ($n_1 = 3.57$) and AlAs ($n_2 = 2.94$) of widths d_1 and d_2 equal to a quarter wavelength in each medium. The grating is placed in an extended GaAs medium. Calculate and plot the transmittance and reflectance of the grating as functions of N, for $N = 1, 2, \ldots, 10$, at a frequency equal to the Bragg frequency.

7.1-8   Bragg Grating: Angular and Spectral Dependence of Reflectance. Write a computer program based on matrix algebra to determine the wave-transfer matrix and the reflectance of an N-layer alternating-layer dielectric Bragg grating. Use your program to verify the graphs presented in Fig. 7.1-12 and Fig. 7.1-13 for the spectral and angular dependence of the reflectance, respectively.

7.2-1   Gap–Midgap Ratio. Using a Fourier optics approach, determine the Bragg frequency and the gap–midgap ratio for the lowest bandgap of a 1D periodic structure comprising a stack of dielectric layers of equal optical thickness, with $n_1 = 1.5$ and $n_2 = 3.5$, and period $\Lambda = 2\ \mu m$. Assume that the wave travels along the axis of periodicity. Repeat the process for $n_1 = 3.4$ and $n_2 = 3.6$. Compare your results.

7.2-2   Off-Axis Wave in 1D Periodic Medium. Derive equations analogous to those provided in (7.2-24)–(7.2-28) for an off-axis wave traveling through a 1D periodic medium with a transverse wavevector k_x.

7.2-3   Normal-to-Axis Wave in a 1D Periodic Medium. Use the results of Prob. 7.2-2 to show that there are no bandgaps for a wave traveling along the lateral direction of a 1D periodic medium, i.e., for $K = 0$.

7.2-4   Omnidirectional Reflector. A periodic stack of double layers of dielectric materials with $n_1 d_1 = n_2 d_2$, $n_2 = 2n_1$ and $\Lambda = d_1 + d_2$ is to be used as an omnidirectional reflector in air. Plot the projected dispersion relation showing the light line for air (a diagram similar to Fig. 7.2-10). Determine the frequency range (in units of ω_B) for omnidirectional reflection.